


A gatekeeper sympathetic control of lacrimal tear secretion and dry eye onset through the NA-Adra1a-Ucp2 pathway

Received: 2 July 2024

Accepted: 27 May 2025

Published online: 05 June 2025

 Check for updates

Mingli Qu^{1,2,3,8}, Qun Wang^{1,2,3,8}, Xiaofei Bai^{1,2,3}, Jing Feng^{1,2,3}, Sai Zhang^{1,2,3}, Yangyang Zhang^{1,2,3,4}, Qing Chen⁵, Hai Zhu⁶, Hengrui Zhang^{1,2,3}, Qunqin Guo^{1,2,3}, Bin Zhang^{1,2,3}, Shengqian Dou^{1,2,3}, Yujie Qiao^{1,2,3}, Hongwei Wang^{1,2,3}, Yihai Cao⁷, Lixin Xie^{1,2,3,4}✉ & Qingjun Zhou^{1,2,3,4}✉

Tear secretion from the lacrimal gland is essential for maintaining ocular surface homeostasis, and its insufficiency causes aqueous-deficient dry eye. Unlike the well-established parasympathetic neuronal regulation, the role of sympathetic nervous system (SNS) in tear secretion remains controversial. Here, we demonstrate the intact sympathetic innervation in lacrimal gland and its activation under multiple dry eye stresses. Pharmacological, surgical, and genetic blockade of SNS increases tear secretion and alleviates dry eye signs. Mechanistically, SNS-driven noradrenaline (NA) release activates α 1a-adrenergic receptor (Adra1a) in acinar and myoepithelial cells to regulate mitochondrial Ucp2 and tear secretion. Systemic and local delivery of Adra1a antagonists, including silodosin and tamsulosin, improves tear secretion and reduces corneal lesions in multiple dry eye mouse models. In addition, we identify the brain locus coeruleus as an upstream driver orchestrating sympathetic regulation of lacrimal secretion. Overall, these findings reveal a gatekeeper role of SNS in tear secretion and offer potential therapeutic strategies for dry eye disease.

Tears are a complex fluid composed of water, electrolytes, proteins, lipids and metabolites, primarily produced by lacrimal gland, meibomian gland, conjunctival goblet and corneal cells^{1,2}. They form a smoothed three-layer tear film and contribute to moisturizing and protecting the healthy ocular surface^{3,4}. The lacrimal gland, which accounts for 90% of tear volume, is primarily composed of acinar, ductal, myoepithelial cells, and resident immune cells⁵. In response to external sensory and psychogenic stimuli, the acinar cells produce primary lacrimal fluid, followed by fluid modification in ducts and tear secretion to ocular surface by the expelling of myoepithelial cells^{6,7}.

Comparatively, lacrimal fluid was dominantly produced by the acinar cells, while the duct cells were estimated to secrete as much as 30% of tear volume⁸.

The chief neural reflex of tear secretion relies on afferent sensory nerves originating from the ocular surface and efferent autonomic nerves innervating the lacrimal gland⁸. The lacrimal gland is predominantly innervated by parasympathetic nervous system (PSNS), which extends from brain superior salivatory nucleus (SSN) via the intermediate pterygopalatine ganglion^{9–13}. Upon the releasing of neurotransmitter acetylcholine (ACh), it stimulates tear production and

¹Eye Institute of Shandong First Medical University, Qingdao, Shandong, China. ²State Key Laboratory Cultivation Base, Shandong Key Laboratory of Eye Diseases, Qingdao, Shandong, China. ³School of Ophthalmology, Shandong First Medical University, Qingdao, Shandong, China. ⁴Qingdao Eye Hospital of Shandong First Medical University, Qingdao, Shandong, China. ⁵School of Clinical Medicine, Shandong Second Medical University, Weifang, Shandong, China. ⁶Department of Urology, Qingdao Hospital, University of Health and Rehabilitation Sciences, Qingdao, Shandong, China. ⁷Department of Microbiology, Tumor and Cell Biology, Karolinska Institute, Solna, Sweden. ⁸These authors contributed equally: Mingli Qu, Qun Wang. ✉e-mail: lixin_xie@hotmail.com; qjzhou2000@hotmail.com

secretion through interacting with M3 muscarinic acetylcholine receptor (M3AChR) of lacrimal acinar, ductal and myoepithelial cells. Therefore, the combination of chronic desiccating stress and muscarinic receptor antagonist scopolamine administration has been widely used to induce dry eye animal models through reducing tear production and secretion from lacrimal gland^{14,15}.

Abnormal tear volume and composition impair ocular surface homeostasis and cause dry eye diseases, which account for a global prevalence ranging from 5% to 50% among the adult populations^{16,17}. Insufficient lacrimal tear production and secretion is the predominant cause of aqueous deficient dry eye, among which the major risks include aging¹⁸, Sjögren's syndrome¹⁹, parasympathetic nerve damage²⁰ and diabetic mellitus²¹. Most previous studies focused the involvement of PSNS impairment during the onset of aqueous deficient dry eye. Accordingly, intranasal varenicline, the nicotinic acetylcholine receptor agonist, has been recently approved for the treatment of dry eye diseases^{22–26}. However, in comparison of PSNS, the anatomical, physiological and pathological relevance of sympathetic nervous system (SNS) in regulating tear production and secretion remains controversial. Anatomically, previous reports using traditional staining methods described variable density and distribution of sympathetic nerves²⁷. Physiologically, electrical and agonist stimulation showed to promote tear secretion or be ineffective^{28,29}, neither sympathetic nor postganglionic denervation combined with agonist infusion caused tear change³¹. More specially, previous studies using ex vivo lacrimal acini and duct segments revealed the sympathetic regulation of healthy tear secretion^{28,30–32}. However, as the crucial response to dangerous or stressful situations, the in vivo intact pathological role of SNS to dry eye stress and its downstream pathway remains largely unknown, which limits the development of therapeutic strategy for the treatment of dry eye diseases.

In this study, we visualized the intact arborization and distribution pattern of sympathetic nerves at single-fiber resolution through tissue clearing and fluorescence imaging. Importantly, we revealed the pathological role of SNS upon dry eye stress and the downstream NA-Adra1a-Ucp2 signaling pathway in reducing tear production and secretion from lacrimal gland. Accordingly, we validated the effectiveness of FDA-approved Adra1a antagonists silodosin and tamsulosin in the treatment of multiple aqueous deficient dry eye mice. In addition, we identified the noradrenergic neural nucleus of brain-to-lacrimal gland axis that orchestrating the sympathetic control of lacrimal tear secretion. Overall, these results highlight a gatekeeper role of SNS activation in controlling tear secretion and confirm the targeting therapeutic efficiency for treating aqueous deficient dry eye diseases.

Results

Sympathetic nerve distribution in mouse lacrimal gland

To visualize the intact nerve fibers, we isolated mouse extraorbital lacrimal gland and used an optimized clearing-enhanced method for fluorescence imaging³³ (Fig. 1a). The sympathetic innervation was examined by the immunolabeling of tyrosine hydroxylase (TH). Through multiple processes of tissue clearance, the lacrimal gland was optically cleared and became nearly transparent (Fig. 1b). As result, the intact network and arborization pattern of sympathetic nerves was visualized at single-fiber resolution through immunolabeling (Fig. 1c). Subsequently, we performed the co-immunolabeling of TH with vascular endothelial marker CD31, acinar cell marker Mist1, epithelial marker E-cadherin (ECAD), myoepithelial cell marker α SMA, ductal cell marker Axna1 and parasympathetic nerve marker choline acetyltransferase (ChAT). Anatomically, the sympathetic nerves of lacrimal gland were divided into larger bundles travelling along vasculature and small fibers extending to acinar and interstitial areas (Fig. 1c). Specifically, most sympathetic nerve fibers were located adjacently and surrounded the acinar cells and myoepithelial cells, with occasionally

close to the ductal cells (Fig. 1d). Quantification analysis revealed that the density of TH⁺ sympathetic nerves was half of ChAT⁺ parasympathetic nerves (Fig. 1e), consistent with previous descriptions of predominant PSNS innervation in lacrimal gland⁸. In addition, sympathetic nerves expressed synaptophysin (SYP), the marker of synaptic vesicles and presynaptic terminals (Fig. 1f). Therefore, through tissue-clearing and fluorescence imaging, we visualized the intact arborization and identified the distinct distribution patterns of SNS and PSNS innervation in mouse lacrimal gland.

Sympathetic activation in response to dry eye stimuli

The sympathetic nervous system is crucial in the “fight or flight” response to dangerous or stressful situations³⁴. To investigate the change of SNS activity upon dry eye stress, we used the scopolamine (SCOP) and chronic desiccating stress-induced dry eye mouse model (Fig. 2a). As expected, the mice exhibited rapid tear reduction after 3 days (Fig. 2b) and corneal lesions after 7 days of SCOP treatment (Fig. 2c, Supplementary Fig. 1a). Concurrently, the number of c-FOS⁺ TH⁺ neurons in the sympathetic superior cervical ganglion (SCG) of dry eye mice was 12-fold higher than that of control mice (Fig. 2d). Patch clamp recordings of SCG neurons with retrograde labeling from lacrimal gland revealed the increased action potential firing rate (Fig. 2e). More importantly, both NA concentration and sympathetic nerve density were elevated in the lacrimal gland of dry eye mice after 7 days of SCOP treatment (Fig. 2f, g), accompanied with reduced ACh concentration and ChAT protein expression (Fig. 2f, Supplementary Fig. 1b). In addition, the dry eye mice exhibited the upregulated expressions of neurotrophic factor *Ngf* and *Gdnf* in lacrimal gland (Fig. 2h), which reported to attract sympathetic nerve growth^{35–37}. Taken together, these findings demonstrated that scopolamine and desiccating stress treatment induced the SNS activation of lacrimal gland, indicating its potential involvement in regulating tear reduction and dry eye onset.

Activated SNS secretes NA to reduce tear secretion of dry eye mice

To elucidate the role of SNS activation in regulating lacrimal tear secretion, we further utilized chemical and surgical denervation in the SCOP-induced dry eye mice (Fig. 3a). The denervation of 6-OHDA and superior cervical ganglionectomy (SCGx) treatment was confirmed by the reduced SNS density and NA concentration in lacrimal gland (Supplementary Fig. 2a). Consequently, tear secretion was markedly increased by 1.9 and 2.2 folds in the 6-OHDA and SCGx-treated mice after 7 days of scopolamine treatment (Fig. 3b), while corneal lesions were ameliorated with both SNS denervation (Fig. 3c). To specifically eliminate sympathetic nerves, we bred *Th*-cre mice with ROSA26i-DTR mice to generate *Th*-DTR mice, which ablated TH⁺ neurons and nerves upon diphtheria toxin (DT) administration (Fig. 3d) as previous descriptions³⁸. The DT-treated *Th*-DTR mice was confirmed with the reduced SNS density and NA concentration in lacrimal gland (Supplementary Fig. 2b). When exposed to scopolamine and chronic desiccating stress treatment, the DT-treated *Th*-DTR mice exhibited the improved tear secretion (Fig. 3e) and corneal lesions (Fig. 3f) than vehicle treatment. Similar results were obtained in the mice pretreated with guanethidine (Fig. 3d–f), which blocks NA release from sympathetic nerve terminals^{39,40}. Overall, these loss-of-function experiments suggest that SNS denervation and blockage increases lacrimal tear secretion of dry eye mice.

To validate the direct contribution of SNS-secreted NA in regulating tear secretion, we conducted a gain-of-function experiment by infusing NA or injecting Adra1a agonist A61603 in the dry eye mice pretreated with 6-OHDA (Fig. 3g). Compared with vehicle-treated mice, the mice with either NA infusion or A61603 injection reproduced the dry eye phenotype of reduced tear secretion (Fig. 3h) and aggravated corneal lesions (Fig. 3i), similar with those observed in the dry

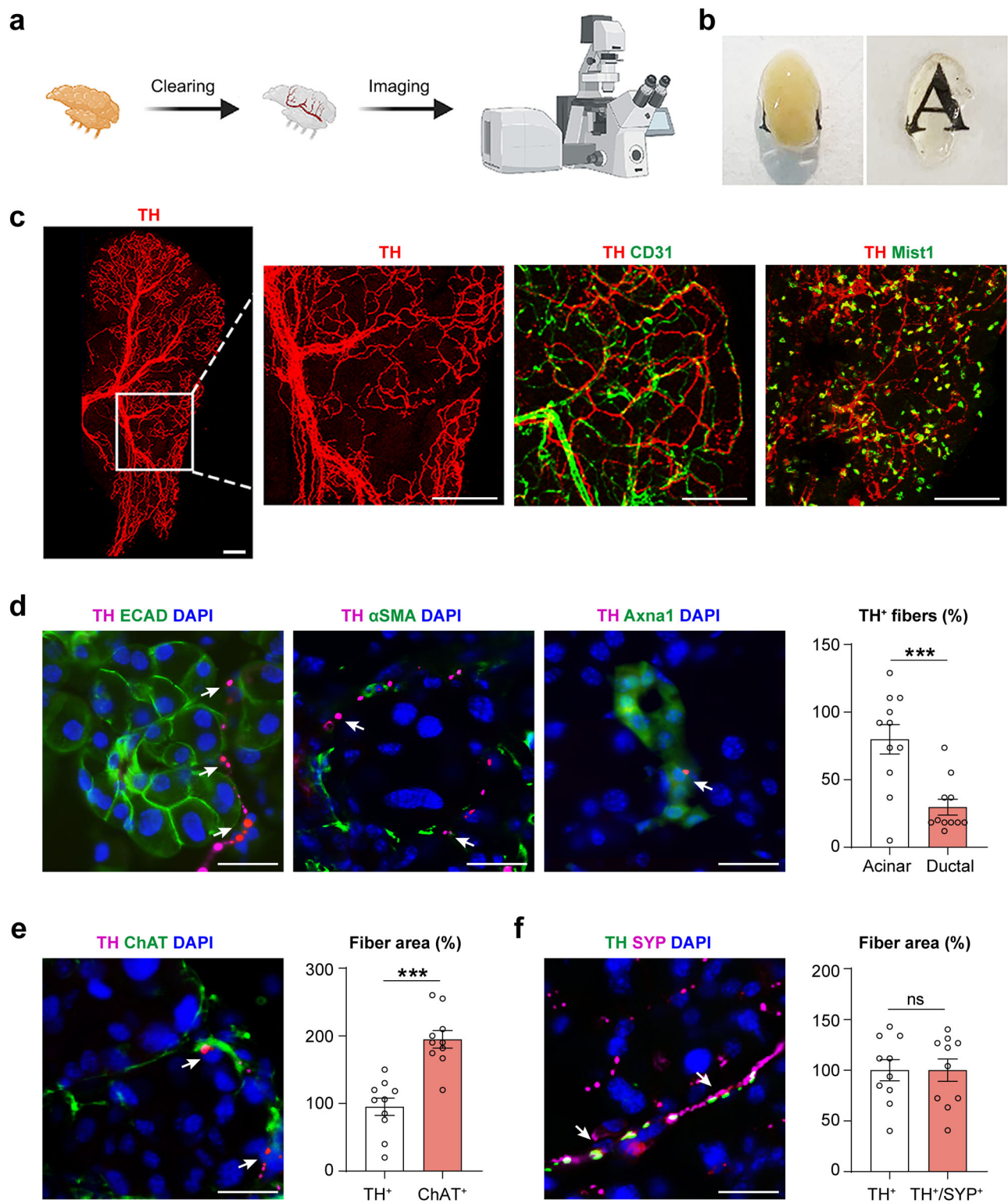


Fig. 1 | Visualization of sympathetic nerves in mouse lacrimal gland.
a Schematic diagram of tissue clearing and fluorescence imaging. Created in BioRender. Wang, Q. (2025) <https://BioRender.com/9ijvlqg>. **b** Lacrimal gland before (left) and after (right) tissue clearing. **c** Representative images of immunolabeling by anti-TH with anti-CD31 and anti-Mist1. Scale bar, 200 μ m. The experiment was repeated at least three times independently with a similar result. **d** Representative images of immunolabeling using anti-TH with anti-E-cadherin (ECAD), anti- α SMA and anti-Axna1. Distribution analysis of TH⁺ nerve fiber density in acinar and ductal area of lacrimal gland ($n = 11$ mice per group, $P = 0.0006$). Scale

bar, 20 μ m. **e** Representative image and quantitative analysis of immunolabeling using anti-TH and anti-choline acetyltransferase (ChAT) ($n = 10$ mice per group, $P < 0.0001$). Scale bar, 20 μ m. **f** Representative image and quantitative analysis of immunolabeling using anti-TH and anti-synaptophysin (SYP) ($n = 10$ mice per group, $P > 0.9999$). Scale bar, 20 μ m. All white arrows indicate TH-labeled sympathetic nerves. Data are shown as mean \pm SEM. The significance of differences was detected using unpaired two-sided Student's t test (**d-f**). *** $P < 0.001$, ns, not significant. Source data are provided as a Source Data file.

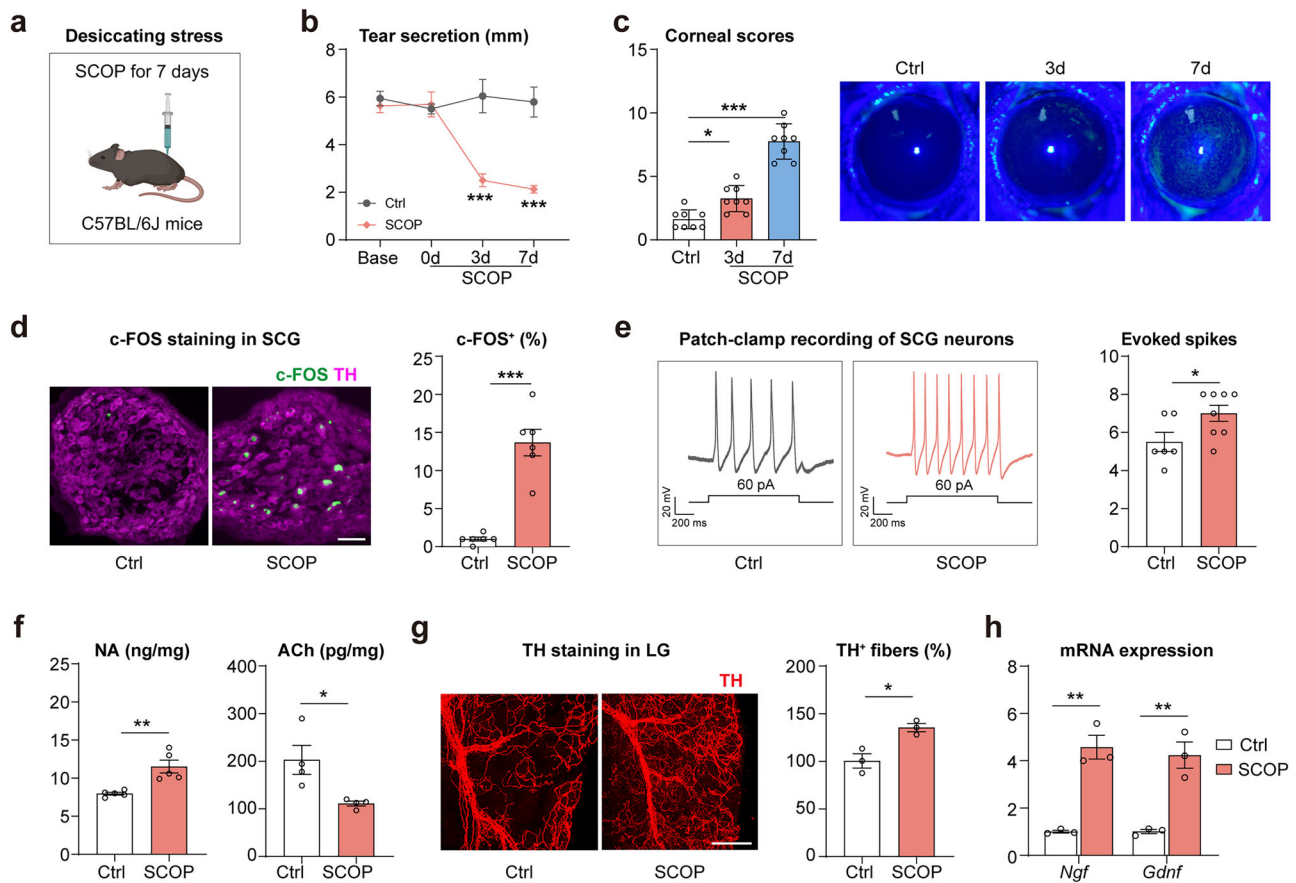


Fig. 2 | Lacrimal SNS activation in response to dry eye stimuli. a Schematic diagram of dry eye mouse model. Created in BioRender. Wang, Q. (2025) <https://BioRender.com/vuq9hqj>. Adult C57BL/6J mice were treated with chronic desiccating stress and scopolamine injection (SCOP, 0.5 mg/0.2 ml, three times per day) for 7 days. **b** Changes of tear secretion ($n = 8$ mice per group. 3 d $P = 0.0003$, 7 d $P < 0.0001$). **c** Changes of corneal fluorescein staining ($n = 8$ mice per group. 3 d $P = 0.0132$, 7 d $P < 0.0001$). **d** Representative images of immunolabelling using anti-TH and anti-c-FOS and quantitative analysis of SCG neurons after 2 h of scopolamine injection ($n = 6$ mice per group. $P < 0.0001$). Scale bar, 50 μ m. **e** Representative patch-clamp recording and quantification of action potential

frequency of retrogradely-labeled SCG neurons from lacrimal gland after 2 h of scopolamine injection (Ctrl: $n = 6$ cells, SCOP: $n = 8$ cells. $P = 0.0353$). **f** NA ($n = 5$ mice per group. $P = 0.0031$) and ACh ($n = 4$ mice per group. $P = 0.0251$) concentrations of lacrimal glands. **g** Representative images of immunolabelling using anti-TH in lacrimal gland ($n = 3$ mice per group. $P = 0.0151$). Scale bar, 200 μ m. **h** Quantitative PCR analysis ($n = 3$ mice per group. Ngf $P = 0.0022$, $Gdnf$ $P = 0.0046$). Data are shown as mean \pm SEM. The significance of differences was detected using unpaired two-sided Student's t test (**b**, **d**, **f**, **g**, **h**), two-sided Mann-Whitney U test (**e**), and one-way ANOVA followed by Dunnett's test (**c**), $*P < 0.05$, $**P < 0.01$, $***P < 0.001$. Source data are provided as a Source Data file.

eye mice without treatment. In addition, to exclude the potential involvement of adrenal gland-released NA, we employed the adrenalectomized mice for dry eye induction. Although surgical adrenalectomy reduced plasma NA concentration, no improvement of tear reduction was observed in these mice (Supplementary Fig. 3). The results suggest that the NA from SNS, but not from adrenal gland, is directly involved in the tear reduction of dry eye mice.

To directly correlate the SNS denervation-improved tear secretion with functional recovery of lacrimal gland, we further performed transcriptomic and histological analysis of mouse lacrimal gland. The transcriptomic analysis found 79 upregulated and 131 downregulated genes upon 6-OHDA treatment (Fig. 3j). KEGG analysis identified the upregulated genes enriched in the salivary and pancreatic secretion signaling pathways, while the downregulated genes enriched in the IL-17 and TNF signaling pathways (Fig. 3k). Quantitative PCR confirmed the upregulated *Prb1* (encodes basic salivary proline-rich protein 1) and *Amy1* (encodes amylase) transcripts, as well as the downregulated *TNF- α* and *IL-1 β* transcripts in the lacrimal gland with 6-OHDA treatment (Fig. 3l). Taken together, these data suggest that SNS inactivation increases tear secretion through improving the lacrimal gland function of dry eye mice.

Adra1a, but not Adra1d, mediates the SNS-controlled tear reduction

Sympathetic nervous system mainly exerts function through releasing NA and binding to specific adrenergic receptors. Previous ex vivo studies reported the mediation of $\alpha 1$ -adrenergic receptor (Adra1) in tear protein or fluid secretion^{8,32,41,42}. To identify the specific receptor controlling tear secretion in vivo, we first measured the mRNA transcripts of mouse lacrimal gland and identified *Adra1a* as the most predominant receptor, followed by *Adrb1*, *Adrb2* and *Adra1d* (Fig. 4a). To dissect their individual roles, the dry eye mice were pretreated with various adrenergic antagonists, including tamsulosin (*Adra1a* antagonist), BMY7378 (*Adra1d* antagonist) and propranolol (*Adrb1/2* antagonist). The results found that tamsulosin treatment, rather than propranolol or BMY7378, significantly improved tear secretion (Fig. 4b) and corneal lesions (Fig. 4c) of dry eye mice. Furthermore, histochemical staining and single-nucleus RNA sequencing analysis showed that tamsulosin treatment reduced the number of macrophages, dendritic cells, and NK cells in lacrimal gland (Supplementary Fig. 4a-c). Quantitative PCR further validated the reduced inflammation in both lacrimal gland and cornea with tamsulosin treatment (Supplementary Fig. 4d, e). The dominant role

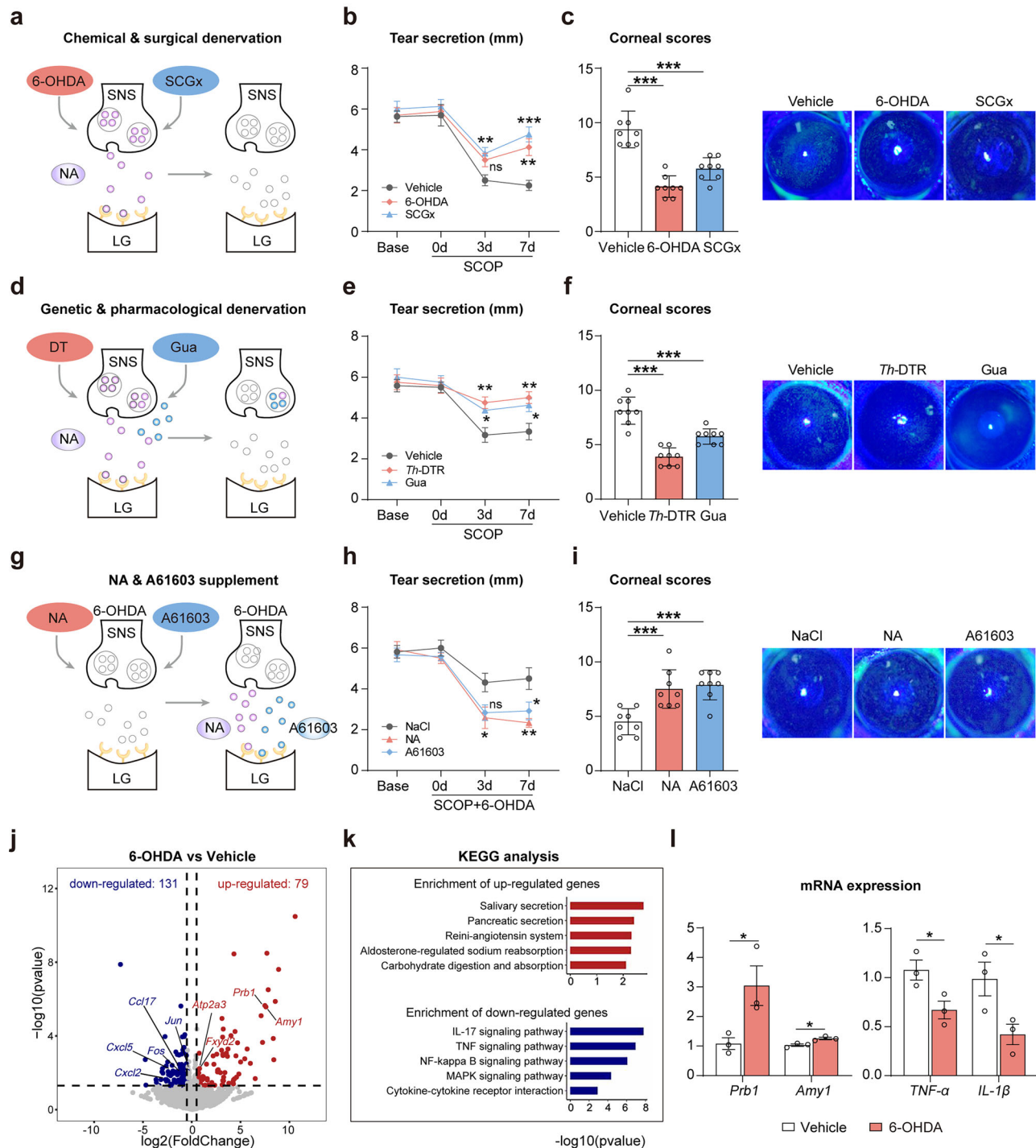
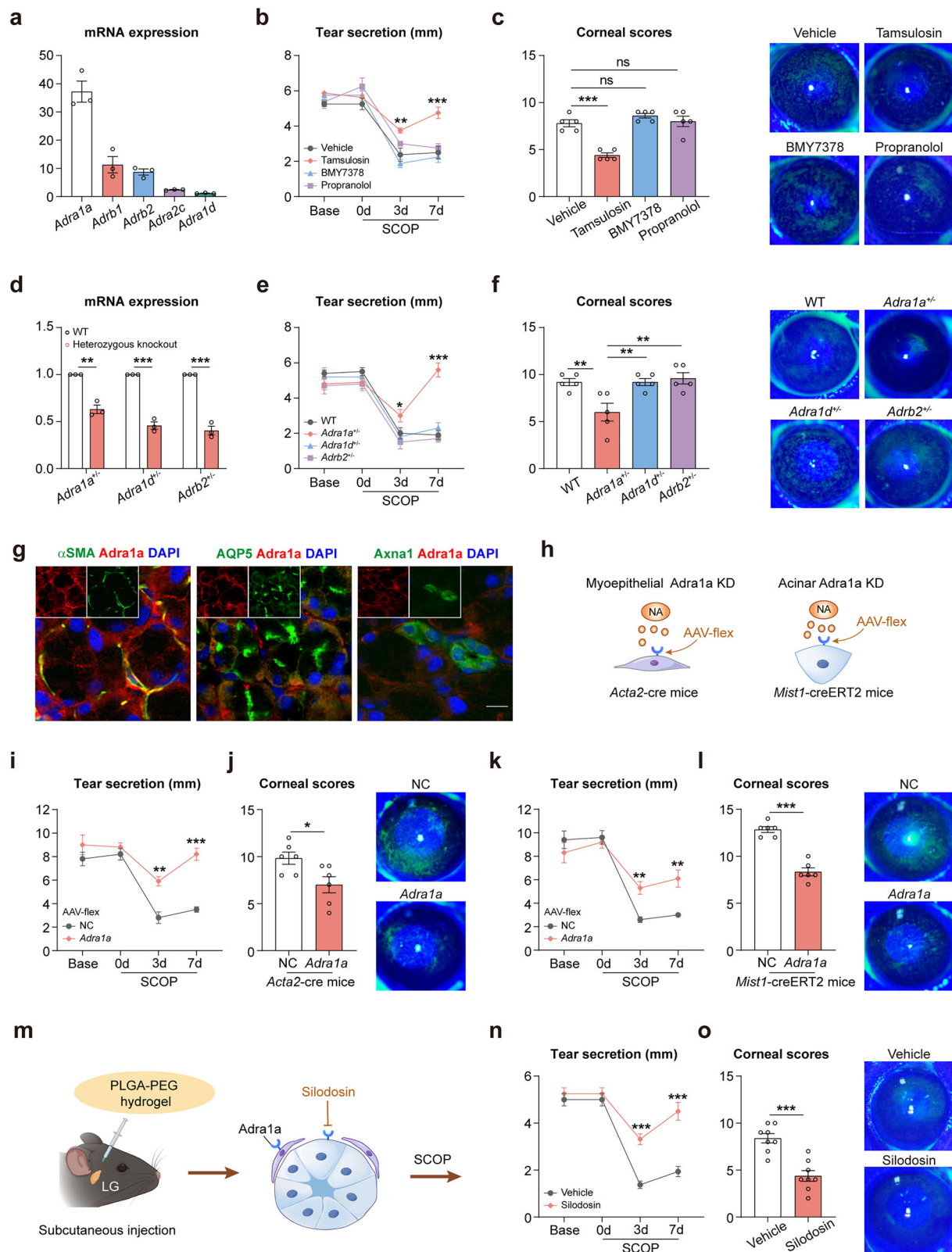


Fig. 3 | SNS inactivation increases tear secretion of dry eye mice. a Schematic diagram of dry eye mice with 6-OHDA and SCGx treatment. Created in BioRender. Wang, Q. (2025) <https://BioRender.com/xa8jatx>. **b** Changes of tear secretion ($n = 8$ mice per group. 3 d 6-OHDA vs Vehicle $P = 0.0501$, SCGx vs Vehicle $P = 0.0100$, 7 d 6-OHDA vs Vehicle $P = 0.0020$, SCGx vs Vehicle $P = 0.0001$). **c** Changes of corneal fluorescein staining ($n = 8$ mice per group. 6-OHDA vs Vehicle $P < 0.0001$, SCGx vs Vehicle $P < 0.0001$). **d** Schematic diagram of *Th*-DTR mice treated with DT and wild type mice with guanethidine (Gua). Created in BioRender. Wang, Q. (2025) <https://BioRender.com/57rh5q8>. **e** Changes of tear secretion ($n = 6$ mice per group. 3 d *Th*-DTR vs Vehicle $P = 0.0016$, Gua vs Vehicle $P = 0.0148$, 7 d *Th*-DTR vs Vehicle $P = 0.0033$, Gua vs Vehicle $P = 0.0154$). **f** Changes of corneal fluorescein staining ($n = 8$ mice per group. *Th*-DTR vs Vehicle $P < 0.0001$, Gua vs Vehicle $P = 0.0001$). **g** Schematic diagram of 6-OHDA and scopolamine (SCOP)-pretreated mice with noradrenaline (NA) or Adra1 agonist A61603 infusion. Created in BioRender. Wang, Q. (2025) <https://BioRender.com/50I00lu>. **h** Changes of tear secretion (NaCl: $n = 8$

mice, NA or A61603: $n = 6$ mice, 3 d NA vs NaCl $P = 0.0288$, A61603 vs NaCl $P = 0.0627$, 7 d NA vs NaCl $P = 0.0059$, A61603 vs NaCl $P = 0.0411$). **i** Changes of corneal fluorescein staining ($n = 8$ mice per group. NA vs NaCl $P = 0.0010$, A61603 vs NaCl $P = 0.0003$). **j** Transcriptomic analysis. Six lacrimal glands from three mice were pooled as one sample, $n = 3$ samples per group. The significance of differential gene expression between two groups is assessed by the Wald test under the negative binomial distribution model. **k** KEGG analysis of the up-regulated and down-regulated genes, the method for calculating P values is based on the hypergeometric distribution. **l** Quantitative PCR analysis ($n = 3$ mice per group. *Prb1* $P = 0.0480$, *Amy1* $P = 0.0199$, *TNF- α* $P = 0.0403$, *IL-1 β* $P = 0.0482$). Data are shown as mean \pm SEM. The significance of differences was detected using one-way ANOVA followed by Dunnett's test at each timepoint (**b, c, e, f, h, i**), and unpaired two-sided Student's t test (**l**), * $P < 0.05$, ** $P < 0.01$, *** $P < 0.001$, ns, not significant. Source data are provided as a Source Data file.



of *Adra1a* was further defined through heterozygous knockout mice (Fig. 4d), among which only *Adra1a*^{+/-} mice, rather than *Adra1d*^{+/-} or *Adrb2*^{+/-} mice, exhibited the improved tear secretion (Fig. 4e) and corneal lesions (Fig. 4f). Collectively, the results of pharmacological treatment and genetic modified mice suggest that *Adra1a*, but not *Adra1d* or *Adrb2*, plays a critical role in the SNS-controlled tear reduction.

Based on the dominant function of *Adra1a* receptor, we next to discrete the roles of SNS in controlling tear production and secretion. Tissue immunolabeling identified the colocalization of *Adra1a* with myoepithelial and acinar cells, but weakly with duct cells (Fig. 4g). Accordingly, we adopted the *Acta2*-cre and *Mist1*-creERT2 mice with the injection of Cre-inducible *Adra1a* interference AAV9 into lacrimal gland (Fig. 4h), which allowed the conditional knockdown of *Adra1a* in

Fig. 4 | Dominant role of *Adra1a* in SNS-controlled tear secretion. **a** mRNA transcripts of adrenergic receptors in mouse lacrimal gland, $n = 3$ samples per group. **b** Changes of tear secretion ($n = 4$ mice per group. 3 d Tamsulosin vs Vehicle $P = 0.0036$, BMY7378 vs Vehicle $P = 0.3396$, Propranolol vs Vehicle $P = 0.1924$, 7 d Tamsulosin vs Vehicle $P = 0.0008$, BMY7378 vs Vehicle $P = 0.8970$, Propranolol vs Vehicle $P = 0.8970$). **c** Changes of corneal fluorescein staining ($n = 5$ mice per group. Tamsulosin vs Vehicle $P < 0.0001$, BMY7378 vs Vehicle $P = 0.3304$, Propranolol vs Vehicle $P = 0.9642$). **d** Verification of expression in the lacrimal gland of *Adra1a*, *Adra1d*, and *Adrb2* heterozygous knockout mice ($n = 3$ mice per group. *Adra1a* $P = 0.0012$, *Adra1d* $P = 0.0002$, *Adrb2* $P = 0.0002$). **e** Changes of tear secretion ($n = 5$ mice per group. 3 d WT vs *Adra1a*^{+/-} $P = 0.1578$, *Adra1d*^{+/-} vs *Adra1a*^{+/-} $P = 0.0773$, *Adrb2*^{+/-} vs *Adra1a*^{+/-} $P = 0.0243$, 7 d WT vs *Adra1a*^{+/-} $P < 0.0001$, *Adra1d*^{+/-} vs *Adra1a*^{+/-} $P < 0.0001$, *Adrb2*^{+/-} vs *Adra1a*^{+/-} $P < 0.0001$). **f** Changes of corneal fluorescein staining ($n = 5$ mice per group. WT vs *Adra1a*^{+/-} $P = 0.0059$, *Adra1d*^{+/-} vs *Adra1a*^{+/-} $P = 0.0059$, *Adrb2*^{+/-} vs *Adra1a*^{+/-} $P = 0.0023$). **g** Representative images of immunolabeling using anti-*Adra1a* with anti- α SMA (myoepithelial cell marker), anti-AQP5

(acinar cell marker) and anti-Axna1 (ductal cell marker). Scale bars, 10 μ m. The experiment was repeated at least three times independently with a similar result. **h** Schematic diagram of conditional knockdown in *Acta2*-cre and *Mist1*-creERT2 mice. Created in BioRender. Wang, Q. (2025) <https://BioRender.com/9ivs458>. **i** Changes of tear secretion ($n = 5$ mice per group. 3 d $P = 0.0012$, 7 d $P < 0.0001$). **j** Changes of corneal fluorescein staining ($n = 6$ mice per group. $P = 0.0252$). **k** Changes of tear secretion ($n = 5$ mice per group. 3 d $P = 0.0018$, 7 d $P = 0.0032$). **l** Changes of corneal fluorescein staining ($n = 6$ mice per group. $P < 0.0001$). **m** Schematic diagram of local silodosin delivery near lacrimal gland. Created in BioRender. Wang, Q. (2025) <https://BioRender.com/q5tdk4d>. **n** Changes of tear secretion ($n = 8$ mice per group. 3 d $P < 0.0001$, 7 d $P < 0.0001$). **o** Changes of corneal fluorescein staining ($n = 8$ mice per group. $P = 0.0001$). Data are shown as mean \pm SEM. The significance of differences was detected using one-way ANOVA followed by Dunnett's test at each timepoint (**b**, **c**, **e**, **f**), and unpaired two-sided Student's *t* test (**d**, **i**, **j**, **k**, **l**, **n**, **o**), * $P < 0.05$, ** $P < 0.01$, *** $P < 0.001$, ns, not significant. Source data are provided as a Source Data file.

the myoepithelial and acinar cells (Supplementary Fig. 5). Following dry eye induction, both knockdown mice exhibited significant improvements of tear secretion and corneal lesions (Fig. 4i–l). Moreover, we purified the acinar cells and myoepithelial cells from mouse lacrimal glands with vehicle- and tamsulosin-treatment. Quantitative PCR confirmed that tamsulosin treatment upregulated tear production-related gene expressions (such as *Aqp5*, *Obp1b*, *Ltf*, and *Lpo*) in the acinar cells, and tear secretion-related gene expressions (such as *Acta2*, *Sparc*, *Atp1a1*, and *Atp1b3*) in the myoepithelial cells (Supplementary Fig. 6). In addition, the measurements of lacrimal blood flow confirmed neither 6-OHDA nor tamsulosin caused apparent changes of blood flow rate (Supplementary Fig. 7). These results suggest that the SNS controls both tear production and secretion through the regulation of lacrimal acinar and myoepithelial cells.

To confirm the specific improvement of systemic *Adra1a* antagonist in lacrimal gland, we designed a local delivery of silodosin using poly (lactic-co-glycolic acid)-polyethylene glycol (PLGA-PEG) hydrogel and injected subcutaneously near lacrimal gland (Fig. 4m). Upon scopolamine and chronic desiccating stress treatment, the mice with local delivery of silodosin exhibited significant improvements of tear secretion (Fig. 4n) and corneal lesions (Fig. 4o). Therefore, through systemic and local antagonist administration, heterozygous knockout and conditional knockdown mice of *Adra1a*, we concluded that SNS activation secreted NA binding to the *Adra1a* receptor of lacrimal acinar and myoepithelial cells to reduce tear production and secretion in response to dry eye stress.

***Adra1a* blockade is effective in multiple aqueous deficient dry eye mice**

Dry eye is a multifactorial disease of different etiology, among which lacrimal gland dysfunction causes the aqueous deficient dry eye diseases¹⁶. To corroborate SNS activation with different aqueous deficient dry eye diseases, we further examined three distinct dry eye mice of Sjögren's syndrome (*TSP-I*^{-/-}), diabetic mellitus and restraint stress with apparent tear reduction and corneal lesions (Fig. 5a–d, Supplementary Fig. 8a–c). These three dry eye mice exhibited similar changes of NA elevation and ACh reduction in lacrimal gland, when compared with their control and wild type mice (Fig. 5a–d). Based on the concurrent SNS activation, we next to explore the popular effectiveness of *Adra1a* blockade for the treatment of multiple aqueous deficient dry eye diseases. The three mice were administrated intraperitoneally with *Adra1a* antagonist tamsulosin (Fig. 5e, h, k). The results revealed that tamsulosin treatment similarly improved tear secretion (Fig. 5f, i, l) and corneal lesions (Fig. 5g, j, m) of the three distinct aqueous deficient dry eye mice. Comparatively, *TSP-I*^{-/-} mice of Sjögren's syndrome exhibited slower improvement of tear secretion, when compared with the mice with diabetes mellitus and restraint

stress. Taken together, these results suggest that the SNS activation of lacrimal gland may represent the common mechanism and therapeutic targeting of multiple aqueous deficient dry eye diseases.

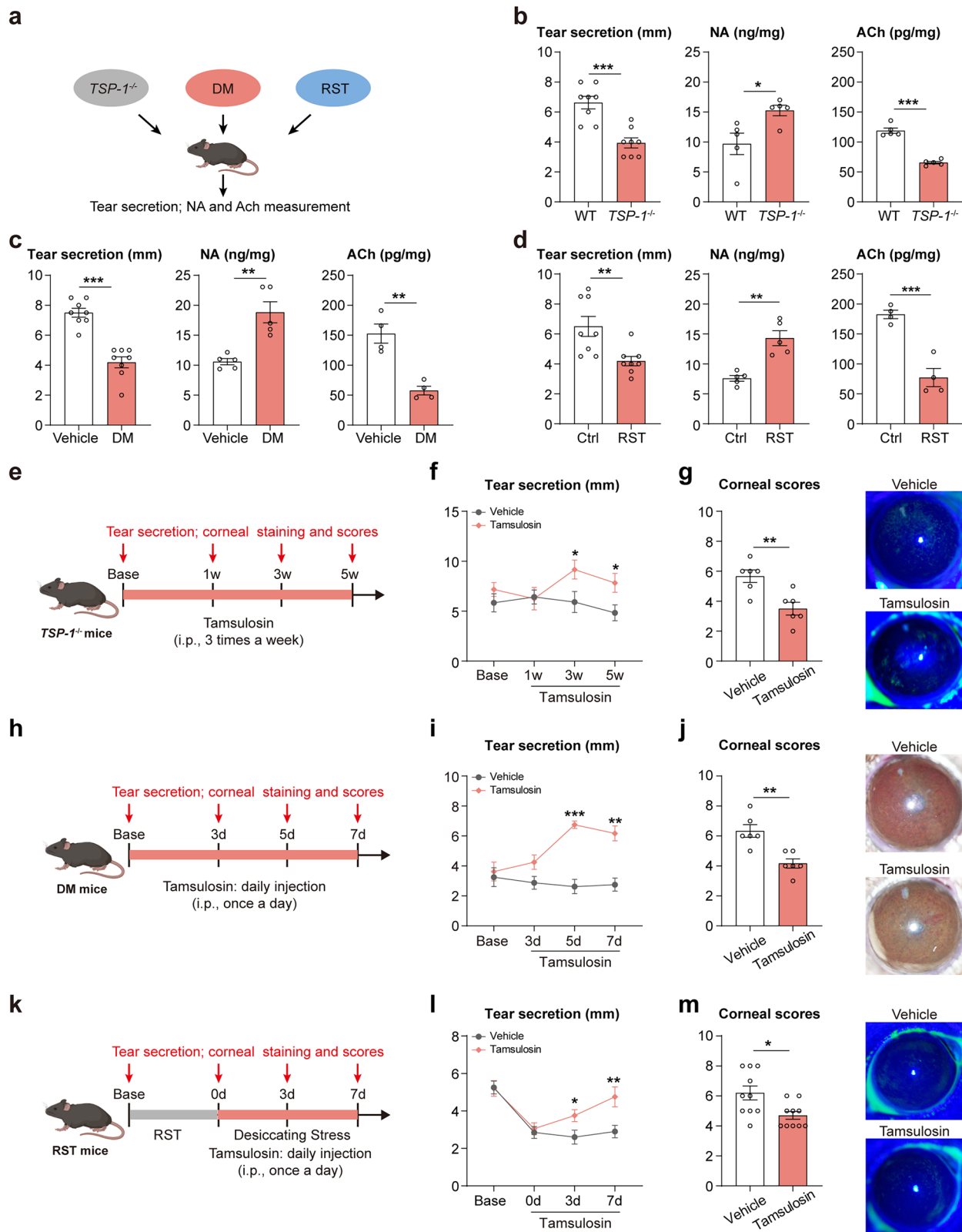
Uncoupling protein 2 governs the SNS-controlled tear secretion

Having identified the dominant role of *Adra1a*, we next to explore the downstream pathway that responds to SNS activation of controlling tear secretion from lacrimal gland. Previous studies have confirmed that uncoupling proteins (Ucp) can be triggered by SNS activation and regulate thermogenesis and insulin secretion^{43–47}. Therefore, we first compared mRNA and protein levels of Ucp1–3 and confirmed the dominant expression of Ucp2 in mouse lacrimal gland (Fig. 6a, b). The scopolamine and chronic desiccating stress treatment induced a rapid and persistent upregulation of Ucp2 compared with Ucp1 and Ucp3 (Supplementary Fig. 9a). Further immunolabeling confirmed the colocalization of Ucp2 with both myoepithelial and acinar cell (Fig. 6c), similar with the localization of SNS and *Adra1a* in lacrimal gland.

To define the involvement of Ucp2 in SNS-controlled tear secretion, we adopted the dry eye induction in C57BL/6J mice pretreated with Ucp2 inhibitor genipin and in *Ucp2*^{-/-} mice (Fig. 6d). Consistent with the reduction of Ucp2 expression in lacrimal gland (Supplementary Fig. 9b–d), both genipin-pretreated mice and *Ucp2*^{-/-} mice exhibited significantly improved tear secretion (Fig. 6e, g) and corneal lesions (Fig. 6f, h), when compared with vehicle-pretreated or wild-type mice. More specifically, we injected the *Ucp2*-interference AAV (shUcp2) into lacrimal gland and followed by dry eye induction. As expected, *Ucp2* knockdown similarly led to the improved tear secretion and corneal lesions (Fig. 6i, j, Supplementary Fig. 9e), accompanied with the elevated mitochondrial maximal and spare respiration capacity, and DNA copy number (Fig. 6k–m). Collectively, these results suggest that the Ucp2 of lacrimal gland governs the SNS-controlled tear secretion in response to chronic dry eye stress.

Brain locus coeruleus involves the SNS-controlled tear reduction

To identify the brain region of projecting noradrenergic output to lacrimal gland, we conducted retrograde trans-synaptic tracing by injecting EGFP-expressing recombinant pseudorabies virus (PRV) into lacrimal gland and mRFP-expressing PRV into SCG (Fig. 7a). At day 2 post PRV injections, only GFP signals were detected in the superior salivatory nucleus (SSN), which was known to convey parasympathetic signals to the lacrimal gland⁹. At day 3, the GFP and mRFP double-labeled signals were distinctly observed in the locus coeruleus (LC), nucleus tractus solitarius (NTS) and paraventricular nucleus (PVN). At day 4, the double-labeled signals became stronger in LC, NTS and PVN, and further detected in the central medial amygdala and paraventricular nucleus, lateral preoptic area (Fig. 7a, Supplementary Fig. 10). Moreover, most LC neurons with double-labeled signals



expressed TH, while SSN neurons with only GFP signals expressed ChAT (Supplementary Fig. 11). These results suggest that the SSN and LC, NTS, PVN may represent the primary brain regions of projecting parasympathetic and sympathetic signals to the lacrimal gland.

Locus coeruleus has been reported to regulate systemic sympathetic outflows^{48,49}. To address the potential role of LC in SNS-controlled tear secretion, we checked and revealed the increased

c-FOS⁺ cells in LC and SSN (Fig. 7b, c), as well as more bursts of action potentials in LC (Fig. 7d) of mice with scopolamine treatment. These results suggest that scopolamine triggered the concurrent activation of sympathetic LC and parasympathetic SSN neurons. Therefore, we employed chemogenetic and optogenetic inhibition of LC adrenergic neurons and monitored the change of tear secretion. We injected Cre-dependent AAV9 encoding mutated human M4 muscarinic receptor

Fig. 5 | SNS activation and effectiveness of Adra1 antagonist in multiple dry eye mice. **a** Schematic diagram of *TSP-1*^{+/−}, diabetic mellitus (DM) and restraint stress (RST)-induced dry eye mice. Created in BioRender. Wang, Q. (2025) <https://BioRender.com/38dm4hu>. **b** Tear secretion, lacrimal NA and ACh concentrations of *TSP-1*^{+/−} mice (tear secretion: *n* = 8 mice, *P* = 0.0002. NA and ACh concentrations: *n* = 5 mice, NA *P* = 0.0241, ACh *P* < 0.0001). **c** Tear secretion, lacrimal NA and ACh concentrations of DM mice (tear secretion: *n* = 8 mice, *P* < 0.0001. NA concentrations: *n* = 5 mice, *P* = 0.0020. ACh concentrations: *n* = 4 mice, *P* = 0.0016). **d** Tear secretion, lacrimal NA and ACh concentrations of RST mice (tear secretion: *n* = 8 mice, *P* = 0.0073. NA concentrations: *n* = 5 mice, *P* = 0.0010. ACh concentrations: *n* = 4 mice, *P* = 0.0008). **e** Schematic diagram of Adra1 antagonist tamsulosin in *TSP-1*^{+/−} mice. Created in BioRender. Wang, Q. (2025) <https://BioRender.com/8074fyf>. **f**, Tear secretion of *TSP-1*^{+/−} mice (*n* = 6 mice per group. 1w *P* = 0.9023, 3w *P* = 0.0445,

5w *P* = 0.0354). **g** Corneal fluorescein staining and scores of *TSP-1*^{+/−} mice (*n* = 6 mice per group. *P* = 0.0048). **h** Schematic diagram of Adra1 antagonist tamsulosin in DM mice. Created in BioRender. Wang, Q. (2025) <https://BioRender.com/mcqp7iu>. **i**, Tear secretion of DM mice (*n* = 4 mice per group. 3 d *P* = 0.0758, 5 d *P* = 0.0003, 7 d *P* = 0.0020). **j** Corneal fluorescein staining and scores of DM mice (*n* = 6 mice per group. *P* = 0.0020). **k** Schematic diagram of Adra1 antagonist tamsulosin in RST mice. Created in BioRender. Wang, Q. (2025) <https://BioRender.com/74k1x4r>. **l**, Tear secretion of RST mice (*n* = 10 mice per group. 0 d *P* = 0.6622, 3 d *P* = 0.0303, 7 d *P* = 0.0087). **m** Corneal fluorescein staining and scores of RST mice (*n* = 10 mice per group. *P* = 0.0117). Data are mean ± SEM. The significance of differences was detected using unpaired two-sided Student's *t* test (**b–d**, **f**, **g**, **i**, **j**, **l**, **m**), **P* < 0.05, ***P* < 0.01, ****P* < 0.001. Source data are provided as a Source Data file.

(hM4Di) into the LC of *Th*-cre mice (Fig. 7e, Supplementary Fig. 12). Consistent with the reduced c-FOS⁺ TH⁺ cells (Fig. 7f) and suppressed activity and excitability of LC neurons (Fig. 7g), the *Th*-cre mice with CNO administration exhibited the elevated tear secretion (Fig. 7h). In addition, we injected Cre-dependent AAV9 encoding eNPHR3.0-EYFP in the LC of *Th*-cre mice for optogenetic inhibition of LC adrenergic neurons (Fig. 7i, j). The mice with optogenetic LC inhibition similarly improved tear secretion within stimulation period (Fig. 7k). Taken together, these findings suggest that LC is represented as a crucial sympathetic brain nucleus of controlling tear secretion from lacrimal gland.

LC-SCG-LG axis regulates reflex tear secretion

Based on the identification of locus coeruleus-superior cervical ganglion-lacrimal gland axis, we next explore its role in regulating reflex tear secretion, which needs the response to external stimuli and convey efferent signals to the lacrimal gland. We adopted the mouse models of corneal nylon thread irritation and intraperitoneal carbachol injection with rapid reflex tear secretion. We bilaterally injected the Cre-dependent AAV9 encoding mutated human M3 muscarinic receptor (hM3Dq) into the LC of *Th*-cre mice (Fig. 8a). Immunofluorescence staining and electrophysiological measurements confirmed the viral infection efficiency and LC neuronal activation upon CNO administration (Fig. 8b, c, Supplementary Fig. 13). The elevation of reflex tear secretion was completely abolished in mice with corneal irritation (Fig. 8d) and partially reduced in mice with carbachol injection (Fig. 8e). In addition, upon peripheral SNS ablation through SCGx (Fig. 8f), the elevation of reflex tear secretion was further enhanced in mice with corneal irritation (Fig. 8g) and prolonged in mice with carbachol injection (Fig. 8h). Overall, these results suggest that the LC-SCG-LG axis also plays a vital role in the precise control of reflex tear volume and period to prevent hypersecretion.

Discussion

Tear secretion is a precise-controlled neural response to various external sensory and psychogenic stimuli^{8,50}. These stimuli are integrated and processed in central nervous system, which sends sympathetic and parasympathetic efferent signals to control tear production and secretion from lacrimal gland. In this study, we visualized the intact arborization of sympathetic and parasympathetic nerves in mouse lacrimal gland. Importantly, we uncovered the in vivo gatekeeper role of SNS and identified the LC-SCG-LG axis in controlling tear production and secretion upon dry eye stress and reflex stimuli. Mechanistically, we identified that the NA-Adra1a-Ucp2 signaling pathway mediated the SNS-controlled tear production and secretion through regulating acinar and myoepithelial cells. In addition, we confirmed the effectiveness of Adra1a antagonists for the treatment of multiple aqueous deficient dry eye in mice (Fig. 9). These findings not only advance mechanical understanding of tear production and

secretion, but also provide potential prevention and treatment paradigms for dry eye diseases.

The lacrimal gland receives brain parasympathetic and sympathetic signals to control tear production and secretion^{51,52}. To settle the anatomical and functional discrepancy of SNS by previous traditional staining and ex vivo studies, we utilized tissue-clearing method to visualize the intact sympathetic arborization of lacrimal gland. Compared with the dense PSNS nerves in both acinar and ductal area, SNS nerves were sparsely localized with acinar and seldom to ductal area. More importantly, single SNS activation in healthy mice with intact PSNS cannot reduce basal tear secretion and produce dry eye disease (Supplementary Fig. 14). These results may explain the dominant role of PSNS and coordinated role of SNS in controlling basal tear production and secretion through the regulation of acinar and myoepithelial cells. However, for reflex tear secretion, SNS activation reduces the elevated tear volume and period evoked by corneal irritation or carbachol injection. These results indicate that the physiological role of SNS is to control proper reflex tear and prevent hypersecretion upon external stimuli and PSNS activation, which is consistent with the response of SNS to dangerous and stressful situations.

The aqueous-deficient dry eye is caused by insufficient tear production and secretion, which was previously considered due to impaired PSNS of lacrimal gland¹⁶. Considering the crucial role of SNS to various stress³⁴, we found the concurrence of SNS overactivation and PSNS impairment in lacrimal gland of dry eye mice. Through a series of loss-of-function and gain-of-function animal experiments, we confirmed that systemic or local blockage of SNS and its downstream pathways improved tear secretion and dry eye severity. Therefore, the SNS serves as a gatekeeper role of controlling lacrimal tear secretion in response to dry eye stress. In this sense, the higher SNS of lacrimal gland may increase the risk of tear reduction and dry eye onset. This could be particularly relevant in older populations, as epidemiologic studies confirmed that the older age is a significant risk factor of dry eye diseases⁵³, possibly due to the impaired SNS and PSNS balance⁵⁴. Therefore, future studies are warranted to define the correlation of tear secretion and lacrimal SNS activity, which may provide potential strategy for the prevention and treatment of dry eye diseases.

Sympathetic nerves mainly release NA and activate downstream signaling pathways through various adrenergic receptors. Previous studies using ex vivo lacrimal segments found the presence of Adra1d, but not Adra1a or Adra1b^{32,41,42}. Here we confirmed the dominant expression and role of Adra1a, but not Adra1d, in controlling tear secretion and dry eye onset. Although Adra1a is an unconventional adrenergic receptor, previous studies have identified its functions in adipocytes⁵⁵, hepatocytes⁵⁶, and cardiomyocytes⁵⁷. In lacrimal gland, we identified the colocalization of Adra1a and synchronous function of acinar and myoepithelial cells through conditional knockdown mice. These findings indicate that acinar and myoepithelial cells may constitute a functional unit of controlling lacrimal fluid production and

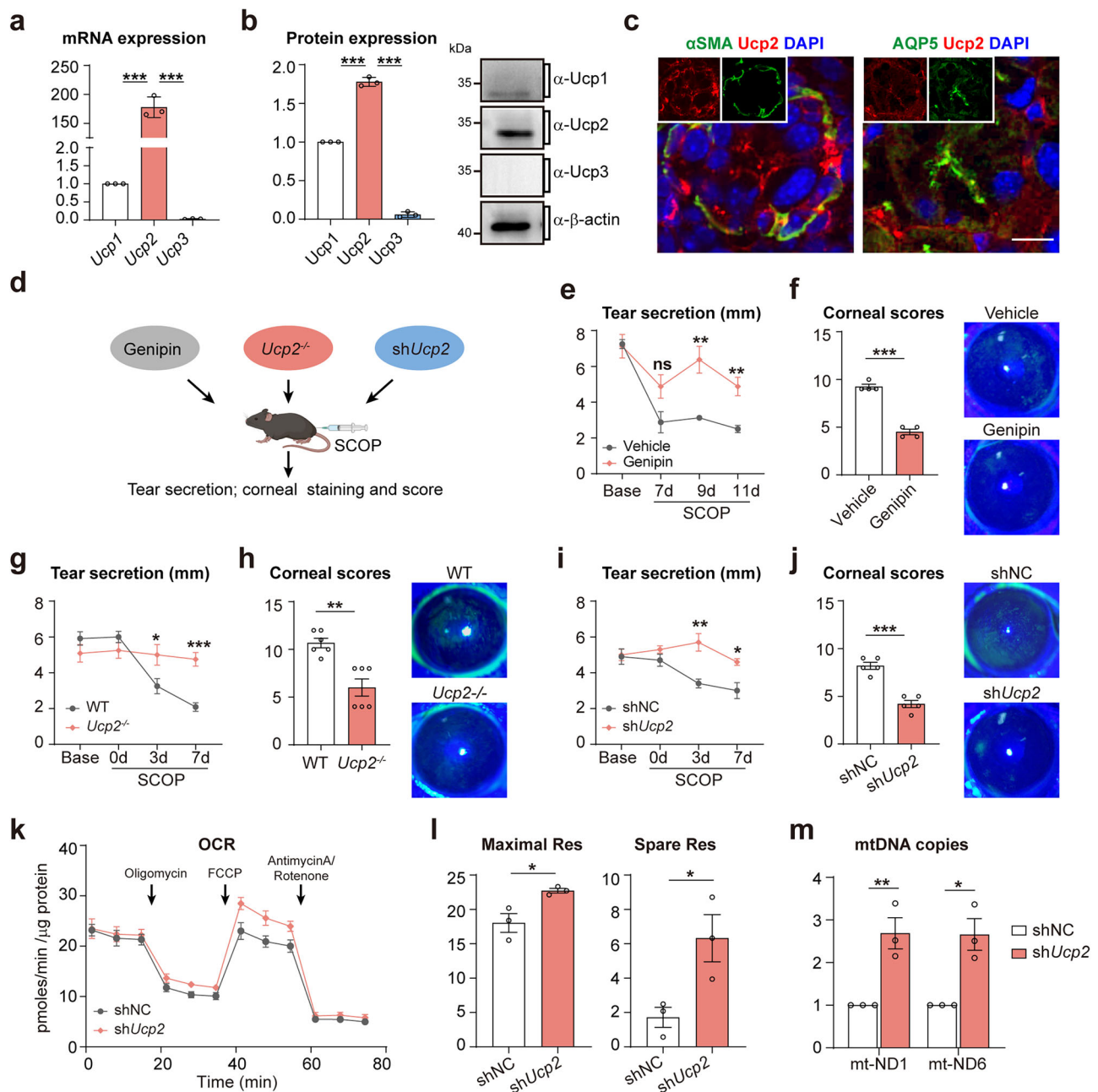


Fig. 6 | Mediation of Ucp2 in SNS-controlled tear secretion. **a** mRNA transcripts of Ucp1-3 in mouse lacrimal gland. ($n = 3$ samples per group. *Ucp1* vs *Ucp2* $P < 0.0001$, *Ucp3* vs *Ucp2* $P < 0.0001$). **b** Proteins of Ucp1-3 in mouse lacrimal gland. (β -actin was used as the Western blot loading control and $n = 3$ replications from three mice. *Ucp1* vs *Ucp2* $P < 0.0001$, *Ucp3* vs *Ucp2* $P < 0.0001$). **c** Representative images of immunolabeling using anti-Ucp2 with anti- α SMA (myoepithelial cell marker), anti-AQP5 (acinar cell marker). Scale bars, 10 μ m. The experiment was repeated at least three times independently with a similar result. **d** Schematic diagram of dry eye mice with genipin treatment, *Ucp2* knockout and *Ucp2*-interference AAV (*shUcp2*) injection into lacrimal gland. Created in BioRender. Wang, Q. (2025) <https://BioRender.com/g5puhqp>. **e** Changes of tear secretion ($n = 4$ mice per group. 7 d $P = 0.0643$, 9 d $P = 0.0051$, 11 d $P = 0.0052$). **f** Changes of corneal

fluorescein staining ($n = 4$ mice per group. $P < 0.0001$). **g** Changes of tear secretion ($n = 6$ mice per group. 3 d $P = 0.0346$, 7 d $P = 0.0001$). **h** Changes of corneal fluorescein staining ($n = 6$ mice per group. $P = 0.0010$). **i** Changes of tear secretion ($n = 5$ mice per group. 3 d $P = 0.0030$, 7 d $P = 0.0108$). **j** Changes of corneal fluorescein staining ($n = 5$ mice per group. $P < 0.0001$). **k**, **l** Mitochondrial oxygen consumption rate (OCR) measurement and analysis. ($n = 3$ samples per group. Maximal Res, $P = 0.0290$, Spare Res, $P = 0.0368$). **m** mtDNA copy number analysis. ($n = 3$ samples per group. mt-ND1, $P = 0.0099$, mt-ND6, $P = 0.0110$). Data are shown as mean \pm SEM. The significance of differences was detected using one-way ANOVA followed by Dunnett's test at each timepoint (**a**, **b**), and unpaired two-sided Student's t test (**e**–**j**, **l**, **m**). * $P < 0.05$, ** $P < 0.01$, *** $P < 0.001$, ns, not significant. Source data are provided as a Source Data file.

secretion into ducts. In addition, we revealed the crucial role of Ucp2 through antagonist treatment, RNA interference and knockout mice. Ucp2 is known to dissipate ATP synthesis coupling by creating proton leakage in mitochondrial inner membrane⁵⁸. Although more functions remain to be defined, previous studies have confirmed the important

roles in glucagon and insulin secretion^{43,44,58}, as well as inflammatory response^{59,60}. It should be mentioned that SNS secrete not only NA, but also ATP, dopamine and oxytocin⁶¹, which may bind to different cells and receptors in the lacrimal gland and evoke multiple effects, including the regulation of tear secretion, blood flow and

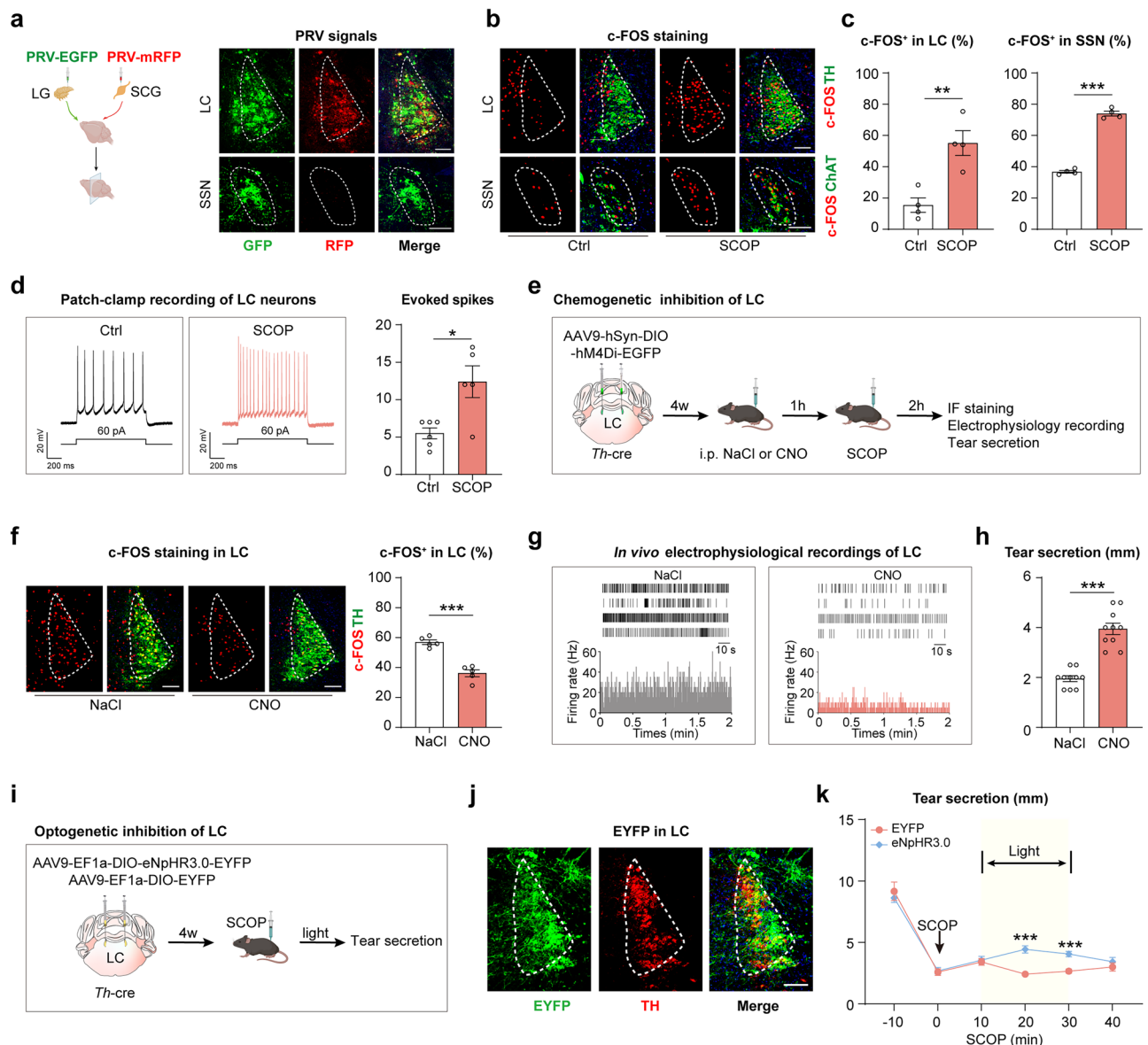


Fig. 7 | Involvement of brain locus coeruleus in the SNS-controlled tear reduction. **a** Schematic diagram of retrograde trans-synaptic tracing and representative images of RFP signals in locus coeruleus (LC) and GFP signals in superior salivatory nucleus (SSN). Created in BioRender. Wang, Q. (2025) <https://BioRender.com/a9nx90z>. Scale bar, 100 μ m. The experiment was repeated at least three times independently with a similar result. **b, c** Representative images and quantitative analysis of c-FOS⁺TH⁺ neurons in LC and c-FOS⁺ChAT⁺ neurons in SSN ($n = 4$ mice per group). LC $P = 0.0050$, SSN $P < 0.0001$. Scale bar, 100 μ m. **d** Representative trace of patch-clamp recording and quantification of action potential frequency under 60 pA current injection for LC neurons in the SCOP-treated mice and vehicle mice (Ctrl: $n = 6$ cells, SCOP: $n = 5$ cells. $P = 0.0476$). **e** Schematic diagram of chemogenetic inhibition in LC of *Th-cre* mice. Created in BioRender. Wang, Q. (2025) <https://BioRender.com/mtcf4so>. **f** Representative images and quantitative analysis of c-FOS⁺TH⁺ neurons in LC after chemogenetic manipulation ($n = 5$ mice per group). $P < 0.0001$. Scale bar, 100 μ m. **g** In vivo electrophysiological recordings of LC neurons in scopolamine-treated hM4Di expressing mice after CNO or NaCl

injection. Representative example rasters (upper panel) and rate histogram (lower panel) of LC neurons in mice treated with CNO or NaCl. **h** Tear secretion of scopolamine-treated hM4Di expressing mice with CNO or NaCl injection ($n = 10$ eyes per group. $P < 0.0001$). **i** Schematic diagram of optogenetic manipulation of LC neurons in *Th-cre* mice. Created in BioRender. Wang, Q. (2025) <https://BioRender.com/mz65rvu>. **j** Neuronal identification of AAV9-EF1a-DIO-eNpHR3.0-EYFP in *Th-cre* mice. The LC noradrenergic neurons (TH) labeled by AAVs (EYFP). Scale bar, 100 μ m. The experiment was repeated at least three times independently with a similar result. **k** Tear secretion of *Th-cre* mice after LC optogenetic manipulation by injecting AAV9-EF1a-DIO-eNpHR3.0-EYFP and control virus (EGFP: $n = 6$ eyes, eNpHR3.0: $n = 8$ eyes. 10 min $P = 0.7374$, 20 min $P = 0.0003$, 30 min $P = 0.0005$, 40 min $P = 0.3973$). The yellow area denotes the inhibition period. Data are shown as mean \pm SEM. The significance of differences was detected using unpaired two-sided Student's *t* test (c, f, h, k) or two-sided Mann-Whitney *U* test (d) * $P < 0.05$, ** $P < 0.01$, *** $P < 0.001$. Source data are provided as a Source Data file.

inflammatory cell infiltration according to current results and previous reports^{62,63}. Therefore, the distinct roles of SNS and its various neurotransmitters in regulating lacrimal gland need further research using specific mouse models.

Dry eye disease is multifactorial and characterized by a vicious cycle of tear film instability and hyperosmolarity. Current therapeutic

strategies include the replacement and stimulation of tear components, as well as anti-inflammation^{64–67}. Recently, the intranasal varicline has been approved to stimulate lacrimal tear secretion via activating trigeminal-parasympathetic pathway^{22–26}. However, the direct strategy of improving lacrimal gland function remains scarce. Here, we identified the pathological role of SNS activation in reducing

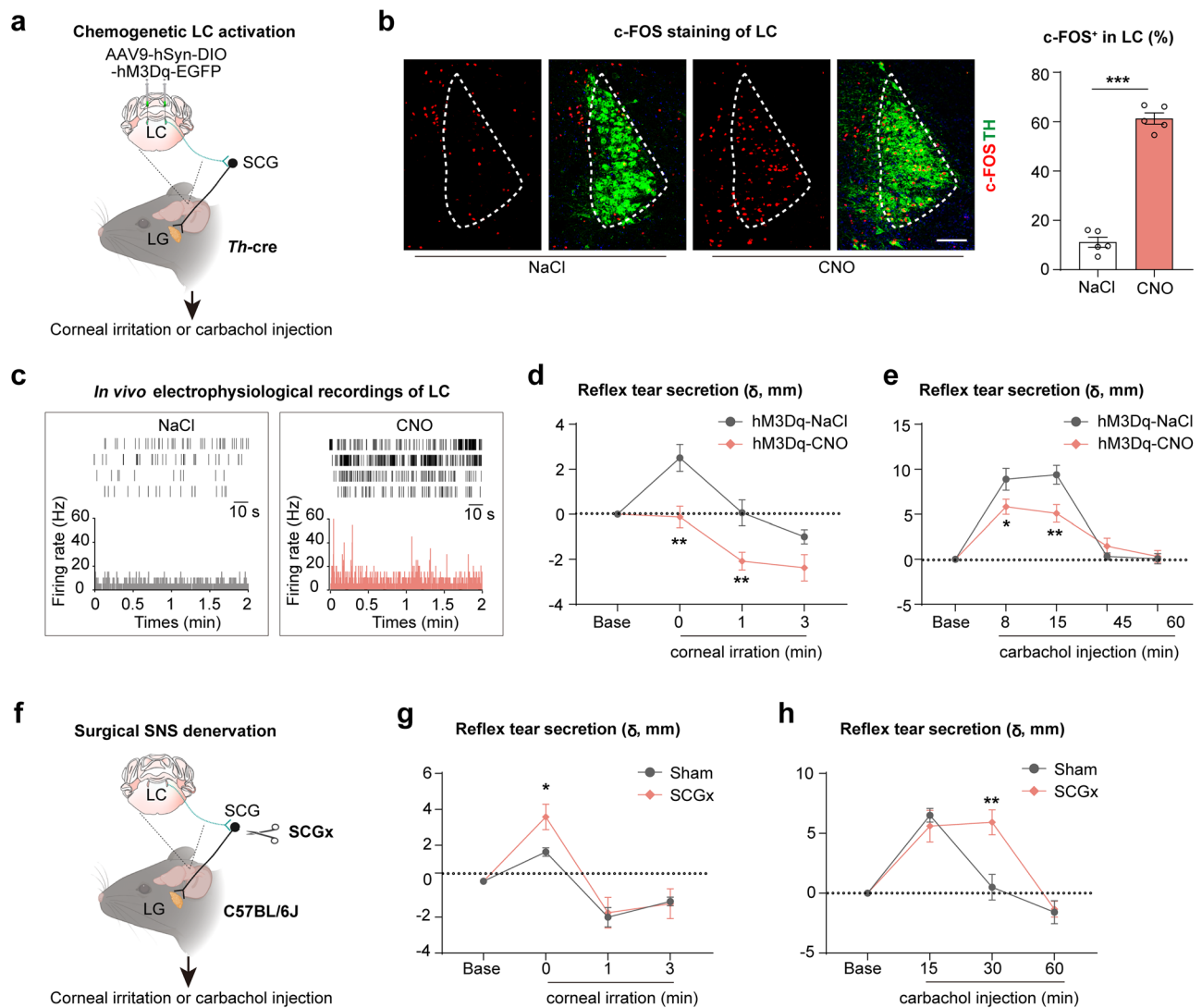


Fig. 8 | Reflex tear secretion with SNS activation and inhibition. **a** Schematic diagram of brain LC activation by AAV9-hSyn-DIO-hM3Dq-EGFP injection in LC of *Th-cre* mice. Created in BioRender. Wang, Q. (2025) <https://BioRender.com/bv59m6f>. **b** Representative images and quantitative analysis of c-FOSTH neurons in LC after chemogenetic manipulation ($n = 5$ mice per group, $P < 0.0001$). Scale bar, 100 μm . **c** In vivo electrophysiological recordings of LC neurons in hM3Dq mice. Representative raster trace (upper panel) and rate histogram (lower panel) of LC neurons in mice 1 hour after CNO or NaCl injection. **d** Dynamics of reflex tear secretion after corneal irritation with nylon thread (hM3Dq-NaCl: $n = 8$ eyes, hM3Dq-CNO: $n = 12$ eyes. 0 min $P = 0.0028$, 1 min $P = 0.0049$, 3 min $P = 0.0905$). **e** Dynamics of reflex tear secretion after carbachol treatment (hM3Dq-NaCl: $n = 8$

eyes, hM3Dq-CNO: $n = 11$ eyes. 8 min $P = 0.0446$, 15 min $P = 0.0088$, 45 min $P = 0.3172$, 60 min $P = 0.7816$). **f** Schematic diagram of SNS ablation by superior cervical sympathectomy (SCGx). Created in BioRender. Wang, Q. (2025) <https://BioRender.com/numw4qn>. **g** Dynamics of reflex tear secretion after corneal irritation with nylon thread ($n = 4$ mice per group, 0 min $P = 0.0397$, 1 min $P = 0.8128$, 3 min $P = 0.8896$). **h** Dynamics of stimulated tear secretion after carbachol treatment ($n = 6$ mice per group, 15 min $P = 0.4523$, 30 min $P = 0.0046$, 60 min $P = 0.8350$). Data are shown as mean \pm SEM. The significance of differences was detected using unpaired two-sided Student's *t* test (**b**, **d**, **e**, **g**, **h**), * $P < 0.05$, ** $P < 0.01$, *** $P < 0.001$. Source data are provided as a Source Data file.

tear secretion through NA-Adra1a-Ucp2 signaling pathway. Based on these findings, several strategies can be developed through pharmacological treatments, such as NA releasing inhibitor guanethidine, Adra1 antagonist prazosin, selective Adra1a antagonist tamsulosin and silodosin, as well as Ucp2 antagonist genipin. Prazosin, tamsulosin and silodosin are FDA-approved commercially available drugs with well-recognized safety for hypertension and prostatic hyperplasia treatment^{68,69}. We designed and demonstrated the efficiency of injectable hydrogel containing silodosin near lacrimal gland, which provides an alternative local route of drug administration. Additional strategies include surgical and chemical SNS denervation, similar with the cardiac and renal sympathetic denervation^{70,71}.

The limitations of our study outline the framework for targeting SNS in controlling tear secretion and treating dry eye diseases. First,

while our findings highlight the potential benefits of Adra1a antagonists in multiple dry eye mice, further clinical validation is necessary through prospective randomized controlled trials. Second, the coordinated mechanisms of SNS and PSNS in regulating tear production and secretion remain to be further elucidated. Additionally, we confirmed the role of SNS activation in restraint stress-induced dry eye mouse model, yet the complex regulation of brain-lacrimal gland axis warrants further investigation, which may link psychological distress with the least recognized emotional tearing and dry eye diseases.

In summary, our results reveal the in vivo gatekeeper sympathetic control of tear secretion from lacrimal gland. The previously unrecognized NA-Adra1a-Ucp2 pathway may provide potential preventive and therapeutic interventions for aqueous deficient dry eye diseases.

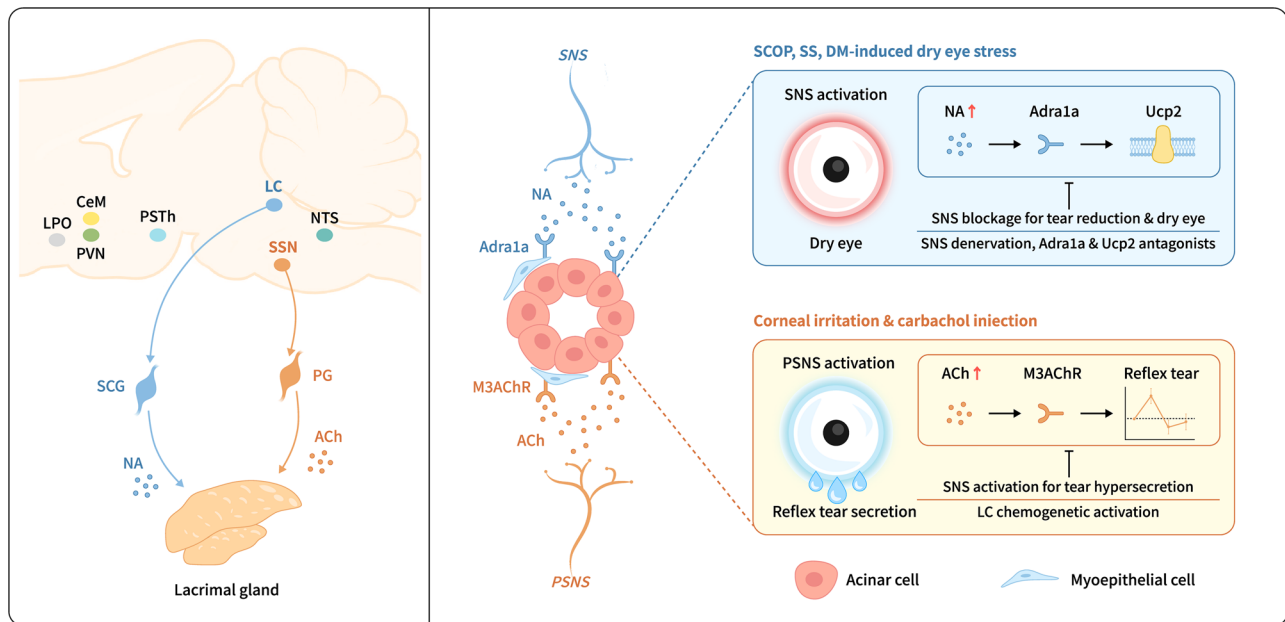


Fig. 9 | Schematic diagram of neural controlled tear secretion from lacrimal gland. Brain locus coeruleus (LC) and superior salivatory nucleus (SSN) represent the central noradrenergic and cholinergic neural nucleus projecting to lacrimal gland via the superior cervical ganglion (SCG) and pterygopalatine ganglion (PG). They release the noradrenaline (NA) and acetylcholine (ACh) that binds to the Adra1a and M₃AChR receptors in the acinar and myoepithelial cells of lacrimal gland. The balanced orchestration of sympathetic nervous system (SNS) and

parasympathetic nervous system (PSNS) precisely controls tear production and secretion from lacrimal gland. Dry eye stress causes SNS activation of lacrimal gland, which reduces tear production and secretion through the NA-Adra1a-UCPs signaling pathway. Corneal irritation and carbachol injection causes PSNS activation, which evokes reflex tear hypersecretion and can be reversed by SNS activation. Created in BioRender. Wang, Q. (2025) <https://BioRender.com/229xwx3>.

Methods

Study approval

The mouse experiments were adhered to the guidelines of the Association for Research in Vision and Ophthalmology (ARVO) and approved by the Ethics Committee of Shandong Eye Institute (no. S-2021-001). Sex was considered in the experimental design and analysis. Female mice were used in general experiments, male mice in the diabetes model, and both sexes in transgenic studies with sex-matched controls.

Mouse strains and breeding

Female C57BL/6J mice were purchased from SPF Biotechnology Co. Ltd. *Th-cre* (T006592), *Adra1a*^{+/−} (T007393), and *Adrb2*^{+/−} (T007691) mice were purchased from GemPharmatech, while ROSA26i-DTR (007900), *Acta2-cre* (029925), and *Mist1-creERT2* (029228) mice were obtained from The Jackson Laboratory. *Adra1d*^{+/−} (NM-KO-190908) and *Ucp2*^{+/−} (NM-KO-00038) mice were purchased from Shanghai Model Organisms Center. *Th-cre* mice were crossed with ROSA26i-DTR mice to obtain *Th-DTR* mice. AAV-flex-*Adra1a* was injected into the lacrimal gland of *Acta2-cre* and *Mist1-creERT2* mice to obtain conditional knockdown mice. Intraperitoneal injection of diphtheria toxin (List labs, #150) at a dose of 0.02 pmol/g of body weight was administered once a day for 13 consecutive days³⁸, while tamoxifen (Macklin, #T832955) was injected at a dose of 75 mg/kg of body weight daily for five days⁷². All mice were maintained under SPF conditions with a 12-hour light/dark cycle at 22 ± 2 °C, and were provided with standard laboratory chow and water ad libitum.

Animal models

The female C57BL/6J mice aged 10–12 weeks were subcutaneously injected with scopolamine hydrobromide (0.5 mg/0.2 ml in PBS; Abcam, #ab141080) three times a day (at 8:00 a.m., 2:00 p.m., and 8:00 p.m.) and placed in the chronic desiccating stress (DS)

environment for 7 consecutive days. For restraint stress (RST), female C57BL/6J mice aged 10–12 weeks were placed into a 50 mL plastic tube 12 h daily for 3 days and subsequently treated with chronic desiccating stress for 7 days. For the Sjögren's syndrome dry eye mouse model, female thrombospondin-1 deficient (*TSP-1*^{−/−}) mice aged 10–16 weeks purchased from the Jackson Laboratory (Bar Harbor, ME, 006141) were used⁷³, with wide-type C57BL/6J mice as control. For the type 1 diabetes mellitus mouse model, male C57BL/6J mice aged 6–8 weeks were intraperitoneally injected with 50 mg/kg streptozotocin (STZ, Sigma, #S0130) for five days. The mice with blood glucose levels higher than 300 mg/dL were used commonly after 16 weeks of the final STZ injection. Mice were euthanized by intraperitoneal injection of sodium pentobarbital (150 mg/kg) following approved institutional protocols.

Tear secretion measurement in mice

For basal tear secretion, the phenol red thread (Jingming, #30059010) was placed on the lower eyelid conjunctiva for 15 sec. The length of wet portion was measured in millimeters⁷⁴. Reflex tear secretion was assessed following corneal irritation with nylon thread or after intraperitoneal (i.p.) injection of carbachol (0.5 mg/kg, MCE, #HY-B1208)¹¹. To minimize the objective operator variation, all mouse tests in this study were performed by the same experienced operator under fixed standardized conditions, including test duration, room humidity and temperature, as well as test time points. In addition, the operator and subsequent analyst were double blind and independently separated to the details of mouse groups.

Corneal staining and scores

Corneal damage was evaluated using two methods: fluorescein staining involved applying 0.25% fluorescein sodium to each eye, rinsing with saline, and imaging with a slit lamp (BQ900, Haag Streit). Rose Bengal staining, for assessing tear film impairment, involved instilling 1% Rose Bengal (Sigma, #330000) and visualization under slit lamp.

The cornea was divided into four quadrants, scored individually, and total score was the sum of these quadrant scores⁷⁵.

Pharmacological inactivation of SNS

For chemical sympathectomy, 6-hydroxydopamine hydrobromide (6-OHDA, Sigma, #162957, 100 mg/kg dissolved in 0.1% ascorbic acid in 0.9% sterile NaCl) were performed by intraperitoneally injection daily for 4 days firstly (from -6 to -3 day), then every 3 days (from -3 to 7 day) during the treatment (a total of 6 injections). To block the release of noradrenaline from sympathetic nerve terminals, guanethidine (Gua, 20 mg/kg, MCE, #HY-B0800) were intraperitoneally injected once daily for 10 days (from -3 to 7 day). To block the adrenergic neurons, β AR antagonist propranolol (2 mg/kg, Sigma, #40543), Adra1a antagonist tamsulosin (0.4 mg/kg, MCE, #HY-B0661), Adra1d antagonist BMY7378 (5 mg/kg, Abcam, #ab120520) were administered by intraperitoneally injection once daily for 7 days. For the other dry eye models, tamsulosin was administrated as daily for 7 days in RST model and diabetes mellitus mice, and for 3 consecutive days every week for 5 weeks in TSP-1^{-/-} mice.

Superior cervical ganglionectomy

Mouse superior cervical ganglionectomy (SCGx) was performed according to previous report⁷⁶. The SCG was gently removed and the incised site was sutured. In the sham group, only skin incisions were made without SCG removal.

Pharmacological activation of SNS

To perform the gain of function experiments, noradrenaline (NA, 0.2 mg/kg per day, MCE, HY-13715A) or the selective Adra1a agonist A61603 (Tocris, #107756-30-9) was performed after pretreatment of 6-OHDA and scopolamine using an implanted osmotic pump (0.24 mL/hour for 7 days; RWD Life Science Co.) or intraperitoneally injection method. The control animals received NaCl as vehicle only.

Formation of silodosin/PLGA-PEG hydrogel

To fabricate the Adra1a antagonist silodosin (MCE, #HY-10122)/PLGA-PEG hydrogel, 1 g of PLGA-PEG (1 g) as a physical crosslinker was added into 4 mL of PBS and incubated at 4°C until the solution achieved clarity. Subsequently, 2.5 mg of silodosin was added to the PLGA-PEG mixture to facilitate the formation of silodosin/PLGA-PEG hydrogel. The resulting thermosensitive hydrogel had a final silodosin concentration of 0.5 mg/mL. As control, a PLGA-PEG hydrogel was prepared by a similar procedure but without silodosin, 60 μ L of PLGA-PEG and silodosin/PLGA-PEG hydrogel precursor solutions were injected subcutaneously around the lacrimal gland to form a gel in situ and assessed for 7 days.

Pharmacologic regulation of Ucp2 activity

To investigate the role of Ucp2 in tear secretion, the mice were orally treated with genipin (50 mg/kg, MCE, #HY-17389), a known inhibitor of Ucp2⁷⁷, 1 h before scopolamine treatment, and then performed every 3 days for 7 days. Saline was used as the negative control.

Whole-mounted immunostaining and tissue clearing

The present procedure was optimized based on the published Ce3D technique³³ and involved the anesthetized mice perfused with phosphate-buffered saline (PBS) containing heparin (10 mg/mL, Sigma, #H3149). The lacrimal gland was subsequently dissected, fixed in 1% PFA at 4°C overnight, and washed with PBS three times. The specified lobe was separated from the lacrimal gland under a dissecting microscope. The samples were permeabilized in 0.2% Triton X-100/20% DMSO and blocked in 0.2% Triton X-100/10% DMSO/5% donkey serum at 37°C for 24 h. The immunostainings were incubated with rabbit anti-TH (1:500, Merck-millipore, #AB152), mouse anti-Mist1 (1:300, Santa, #sc-80984), goat anti-CD31 (1:300, RD, #AF3628) in

0.2% Tween-20/10 mg/mL heparin/5% DMSO/5% donkey serum at 37°C for 72 h, and washed in 0.2% Tween-20/10 mg/mL heparin at 37°C for 1 h five times. The samples were further incubated with secondary antibody conjugated with Alexa Fluor-647, -488 (1:300, Invitrogen, #A32795, #A21202, #A-11055) in 0.2% Tween-20/10 mg/mL heparin/5% donkey serum at 37°C for 48 h, and washed in 0.2% Tween-20/10 mg/mL heparin at 37°C for 2 h five times before the tissue clearing. The samples were cleared with the Ce3D solution (N-methylacetamide (22% w/v), Histodenz (86% w/v), Triton X-100 (0.1% v/v), 1-Thioglycerol (0.5% v/v)) at 37°C for 6 h. The fluorescence imaging was visualized with a LSM880 confocal microscope (ZEISS). Nerve fibers density was analyzed using Image J software (NIH).

Retrograde trans-synaptic PRV tracing

The mice were anesthetized with intraperitoneal injection of 0.6% pentobarbital sodium (10 mg/kg) and the surgical site was cleaned and disinfected with alcohol. PRVs were injected into the lacrimal gland and superior cervical ganglion. To inject PRV-CAG-EGFP (5*10⁹ genomic copies per milliliter, Brain Case, #BC-PRV-531), 1 μ L was slowly injected into multiple lobes of the right-side lacrimal gland through microinjection with uniform speed. An incision was made on the right side of the mouse's neck to expose the SCG, and 1 μ L PRV-CAG-mRFP (1*10⁹ genomic copies per milliliter, Brain Case, #BC-PRV-724) was slowly injected into the SCG. After each injection, the microinjection needle was held in place for 5 minutes, and then the surgical incision was sutured. The mice were kept for 1-4 days for tracking and labeling before being sacrificed.

RNA sequencing and analysis

For performing RNA sequencing, 6 lacrimal glands were pooled as 1 sample from scopolamine-treated and the 6-OHDA plus scopolamine-treated mice, respectively. Each group has 3 samples. RNA-sequencing libraries were prepared using 1 mg of total RNA as input. Total RNA is enriched by oligo(dT) magnetic beads. RNA-seq library preparation using Hieff NGS ClO2PI Ultima Dual-mode mRNA Kit (YEASEN). The completed libraries were qualified with Agilent 2100 Bioanalyzer and sequenced on DNBSEQ platform. Quality control (QC) is performed on the raw reads with SOAPnuke (<https://github.com/BGI-flexlab/SOAPnuke>, version 1.5.2)⁷⁸. The clean reads were aligned to the reference gene sequence (GRCm38.p6) by Bowtie2 (<http://bowtie-bio.sourceforge.net/bowtie2/index.shtml>, version 2.2.5)⁷⁹. Then, RSEM (<http://deweylab.biostat.wisc.edu/rsem/rsem-calculate-expression.html>, version 1.2.8)⁸⁰ was used to calculate the gene expression level of each sample. Differentially expressed genes were calculated with R package DESeq2 (<http://www.bioconductor.org/packages/release/bioc/html/DESeq2.html>, version 1.4.5). KEGG pathway enrichment analysis of differentially expressed genes was performed by clusterProfiler (<https://github.com/YuLab-SMU/clusterProfiler>, version 3.14.3) R package⁸¹. Results were visualized with the ggplot2 (<https://ggplot2.tidyverse.org/>, version 3.3.2) R package.

Laser speckle imaging

A laser speckle imager (LSOI, SIM BFI HR, SIM Opto-Technology Co., Ltd, Wuhan, China.) was used to monitor lacrimal gland blood flow in dry eye mice following the treatments of 6-OHDA or Tamsulosin⁸². The system consisted of a continuous wavelength (λ = 785 nm) laser source, an Olympus ZS61 microscope, a charge-coupled-device camera, and a computer. Briefly, mice were anesthetized by intraperitoneal injection of 0.6% pentobarbital sodium (50 mg/kg), and lacrimal glands were surgically exposed. The monitor detector was set 25–30 cm above the lacrimal glands, with a maximum field of view so that the entire lacrimal gland region could be illuminated. Two-dimensional microcirculation images were captured after the lacrimal gland was exposed and 5 minutes later. For each animal, 10 consecutive images were captured at each time point. For image data

analysis, regions of interest (ROIs) were created on the main vessels of each image. The measurement of blood flow in the LSCI was performed by tools provided by the software, and the values obtained were the average blood-flow values in the region. The vessel diameter was the average of 10 consecutive images from each animal and performed by tools provided by the software.

Neuronal manipulations

For stereotaxic surgery, *Th-cre* mice were anesthetized with pentobarbital sodium and placed in the stereotaxic apparatus (RWD Life Science Co.). The skull was exposed after skin cleaning, and a small hole was drilled into the skull after LC region was located. AAV was injected at 0.12 μL /minute into LC region (coordinates, bregma: AP: -5.41 mm; ML: ± 0.8 mm; DV: -3.75 mm, 200 nL for each site) using a glass micropipette connected to a microsyringe pump. AAV9-hSyn-DIO-hM4Di-EGFP (at $\sim 5.57 \times 10^{13}$ vector genomes per milliliter) and AAV9-hSyn-DIO-hM3Dq-EGFP (at $\sim 3.8 \times 10^{13}$ vector genomes per milliliter) were injected for chemogenetic experiments. AAV9-EF1a-DIO-eNpHR3.0-EYFP (at $\sim 1 \times 10^{13}$ vector genomes per milliliter), AAV9-EF1a-DIO-ChR2-EYFP (at $\sim 1 \times 10^{13}$ vector genomes per milliliter) or AAV9-EF1a-DIO-EYFP (at $\sim 1 \times 10^{13}$ vector genomes per milliliter) were injected for optogenetic experiments. All coordinates were obtained from *Paxinos and Franklin's the Mouse Brain in Stereotaxic Coordinates*. The glass micropipette was kept in place for 10 minutes to ensure virus diffusion after each injection. Mice were allowed to recover for at least 3 weeks. In chemogenetic experiments, Clozapine N-oxide (CNO, Abcam, #ab141704) was injected intraperitoneally at a dose of 1 mg/kg, with 0.9% NaCl used as control. In optogenetic experiments, the ferrule capped optical fiber (200 μm core diameter, NA = 0.37, Hangzhou Newdoon Technology Co. Ltd.) was used and was implanted 0.5 mm above the virus injection site with an angle of 13° (AP: -5.41 mm; ML: ± 0.8 mm; DV: -3.25 mm). Light intensity was measured with a luminometer (PM100D power meter, Thorlabs Inc.). The optogenetic inhibition experiments were conducted by delivering continuous yellow (593 nm) light for a duration of 20 minutes, with final output powers of 1 mW mm^2 . The optogenetic activation experiment was conducted using continuous blue light (465 nm) for 5 minutes, with light parameters set to a 25 Hz pulse frequency and a pulse width of 10 ms. For SCG injection, 2 μL AAV-hSyn-HA-hM3Dq-IRES-mCitrine (at $\sim 2.18 \times 10^{13}$ vector genomes per milliliter) was microinjected. After 3 weeks, CNO or NaCl was injected intraperitoneally.

Electrophysiological recording

For patch clamp recordings of SCG neurons in vitro, AAV/retro-hSyn-EGFP were injected into lacrimal gland retrogradely label the SCG neurons that innervates the lacrimal gland. At least 4 weeks after AAV-injections, SCG neurons were separated for electrophysiological measurements. The SCGs were isolated in HBSS, dissociated using L15 medium containing 2 mg/ml collagenase A for 40 minutes, and subsequently digested in 0.05% trypsin for 30 minutes in a 37°C incubator at 5% CO_2 . The cells were resuspended, plated on a poly-D-lysine coated coverslip and cultured in L15 complete media supplemented with N2, B27, 1% penicillin-streptomycin, 5% FBS. After 24 h, coverslips containing SCG neurons were positioned in a recording chamber and continuously perfused with bath solution (NaCl 140 mM, KCl 4 mM, MgCl_2 2 mM, CaCl_2 5 mM, D-Glucose 5 mM, HEPES 5 mM, pH 7.4).

For patch clamp recordings of LC neurons in vitro, acute brain slices were prepared using vibratome in ice cold slicing solution (NMDG 87 mM, KCl 2.5 mM, NaH_2PO_4 1.2 mM, NaHCO_3 30 mM, HEPES 20 mM, glucose 25 mM, N-acetyl cysteine 12 mM, Na-ascorbate 5 mM, thiourea 2 mM, Na-pyruvate 3 mM, MgSO_4 10 mM, CaCl_2 0.5 mM, pH 7.4). After immersing in slicing solution for 15 minutes at 34°C , slices were transferred to artificial cerebrospinal fluid and stored at room temperature until use. The electrodes were pulled from borosilicate glass micropipette capillaries (BF150-86-10, Sutter, USA) using a

micropipette puller (P-97, Sutter, USA) with resistances ranging from 1.8 to 4 M Ω . The pipette internal solution contained (in mM): potassium gluconate 140 mM, MgCl_2 2 mM, EGTA 1 mM, HEPES 10 mM, Na_2GTP 0.3 mM, Na_2ATP 2 mM, pH 7.4. Electrical signals were acquired using the Axoclamp 700 A amplifier (Axon Instruments, USA), digitized using a Digidata 1440 A (Axon Instruments, USA) interface and recorded with Clampex 10.7 (Axon Instruments, USA) Current-clamp mode was used to record action potentials of SCG and LC neurons. Current injection was held at 0 and evoked for 1 sec.

For electrophysiological assessments of LC neurons in vivo, 8-channel microelectrode arrays were implanted into the LC (coordinates, bregma: AP: -5.41 mm; ML: ± 0.8 mm; DV: -3.75 mm) of anesthetized mice. Extracellular signals were then amplified recorded and band-pass filtered (250 Hz–5 kHz) at 30 kHz sampling rate using an A32-OM32 adaptor connected to a Cereplex digital headstage (Blackrock Microsystems, UT). In the chemical genetic inhibition experiments, after injecting AAV9-hSyn-DIO-hM4Di-EGFP virus into the LC of mice for four weeks, CNO group mice were given a subcutaneous scopolamine injection in the lower limbs after intraperitoneal injection of CNO one hour later. Controls received NaCl before scopolamine injection. Data were collected 3 h after CNO or NaCl injection. In the chemical genetic activation experiments, after injecting AAV9-hSyn-DIO-hM3Dq-EGFP virus into the LC of mice for four weeks, mice were given intraperitoneal injection of CNO or NaCl. Data were collected 1 hour after CNO or NaCl injection. Data were analyzed using Neuroexplorer 5.

AAV generation and administration in lacrimal gland

Mice were injected with AAV, which mediated the efficient transduction of lacrimal gland at $\sim 5 \times 10^{12}$ vector genomes per milliliter. AAV-flex containing the *Adra1a* target interference sequences (TGCCAAGAA-TAAGACTCACTT) and AAV containing the *Ucp2* interference sequences (TCCTTCTCCGCTTGGGAT) were obtained from Genechem. After at least 3 weeks, infection efficiency was detected. For *Acta2-cre* and *Mist1-creERT2* mouse strains, efficiency was detected about 5 weeks post injection. AAV solution at 2 μL was injected using a 36 G beveled needle (World Precision Instruments, #NF36BV-2) mounted on a 10 μL microsyringe (World Precision Instruments, #NanoFil 300,329).

Immunohistochemical staining

Each entire lacrimal gland per mouse was fixed in 10% formalin and paraffin-embedded, sections (4 μm) were incubated with rabbit anti-CD45 (1:50, Abcam; #ab10558) overnight at 4°C and subsequently incubated with secondary antibodies and visualized using DAB detection kit (MXB, #DAB-0031) according to the manufacturer's instructions. Images were captured with a light microscopy (Nikon).

Immunofluorescence staining

For brain and lacrimal gland frozen sections preparation, under deep anesthesia, mice were transcardially perfused with ice-cold PBS, followed by 4% paraformaldehyde (PFA). The brains and lacrimal glands were removed and postfixed with PFA at 4°C overnight and then cryoprotected in 30% sucrose for 48 h. The coronal sections of brains for PRV tracing were sliced at 100 μm , others were sliced at 25 μm . The lacrimal glands sections were sliced at 20 μm . For superior cervical ganglion, samples were embedded in OCT compound and sections of 7 μm were made. Brain sections were immuno-stained with free-floating (100 μm) or slide-mounted (25 μm) manner.

Brain and lacrimal gland sections were incubated in blocking buffer containing 5% donkey serum and 1% BSA and 0.1% Triton-X in PBS for 1 h at room temperature. Sections of SCG were fixed in 4% PFA for 10 minutes and washed with PBS, then incubated in 3% Triton X-100-PBS for 30 minutes and blocked with 5% donkey serum at room temperature. Then sections were incubated with primary antibody diluted in blocking buffer overnight at 4°C . The chicken anti-GFP

(1:300, Abcam, #ab13970), rabbit anti-RFP (1:300, Takara, #632496), mouse anti-TH (1:300, RD, #MAB7566), chicken anti-TH (1:300, Merck-millipore, #AB9702), rabbit anti-c-FOS (1:300, Abcam, #ab222699), mouse anti-CHAT (1:200, Sigma, #AMAB91130), rabbit-anti-CHAT (1:300, invitrogen, PA5-29653) were used as primary antibodies for brain sections. The rabbit anti-TH (1:300, Merck-millipore, #AB152), rat anti-ECAD (1:200, Life technologies, #13-1900), mouse anti- α -SMA (1:300, Abcam, #ab7817), rabbit anti-SYP (1:200, Abcam, #ab32127), sheep anti-TH (1:200, Merck-millipore, #AB1542) mouse anti-CHAT (1:300, sigma, #AMAB91130), goat anti-CD31 (1:200, RD, #AF3628), mouse anti-Adra1a (1:100, Santa, #sc100291), mouse anti-Ucp2 (1:100, Santa, #sc390189), rabbit anti-Aqp5 (1:100, Abcam, #ab78468), rabbit anti- α -SMA (1:300, Abcam, #ab5694), rabbit anti-Axna1 (1:100, Abcam, #ab214486), rabbit anti-Mist1 (1:200, Servicebio, #GB114483) were used as primary antibodies for lacrimal gland sections. The sheep anti-TH (1:200, Merck-millipore, #AB1542) and rabbit anti-cFos (1:200, Abcam, #ab190289) were used as primary antibodies for SCG sections. Alexa dye-conjugated secondary antibodies were from Invitrogen. Sections were mounted and images were taken with a LSM880 confocal microscope (ZEISS) or a fluorescence microscope (Nikon). For quantification of TH and SYP immunoreactivity in lacrimal gland sections, under low-power magnification, 10 randomly selected rectangular areas (30×40 μ m) were chosen. Then, with a 20×objective, the punctate TH and SYP labeling were counted and the results were averaged as the amount of TH or SYP immunoreactivity in lacrimal gland sections. Cell counting of fluorescent images were made with ImageJ software (NIH).

Isolation and purification of acinar and myoepithelial cells

Ten lacrimal glands were collected and digested in a solution containing 2 mg/ml collagenase II (Sigma, C6885) at 37 °C for 1–2 h. The resulting cell suspension was filtered through a 40 μ m cell strainer. To remove erythrocytes, erythrocyte lysis solution (Qiagen, 79217) was added and followed by centrifugation at 300 g for 10 minutes. The cell pellet was treated with Dead Cell Removal Kit (Miltenyi Biotec, #130-090-101) to eliminate dead cells. The living cells were resuspended in MACS buffer (PBS, 0.5% bovine serum albumin, and 2 mM EDTA) and incubated with rabbit anti-Aqp5 (1:100, Abcam, #ab78468) or rabbit anti-CD10 (1:100, Proteintech, #23898-1-AP) for 30 minutes at 4 °C. Following this, samples were washed by adding 2 ml MACS buffer and centrifuged at 300 g for 10 minutes. Then, the cells were incubated with anti-rabbit IgG MicroBeads (Miltenyi Biotec, #130-048-602) for 15 minutes at 4 °C. Bead-labeled cells were separated using MS Separation Columns (Miltenyi Biotec, #130-042-201). The purified acinar and myoepithelial cells were used for RNA extraction and subsequent Quantitative RT-qPCR.

Quantitative RT-qPCR

For tissue, two pooled lacrimal glands from each mouse were collected as one sample. Total RNA was extracted using Nucleospin RNA Kits (Transgen, #ER501-01) and then reverse transcribed into cDNA with the HiScript III RT SuperMix kit (Vazyme, #R333). mRNA expression levels were measured with a 7500 Real-time PCR system (Applied Biosystems) using SYBR green dye (Roche, #04913914001). Primer sequences are listed in Supplementary Table 1.

DNA extraction and mitochondrial DNA (mtDNA) copy number analysis

Total DNA was extracted from lacrimal glands using the Easy Pure genomic DNA kit (Transgenes, #EE101-01) in accordance with the manufacturer's protocol. The copy numbers of NADH dehydrogenase subunits 1 and 6 (mt-ND1 and mt-ND6) were evaluated with β -globin as an internal reference gene. The primer sequences used for amplifying mouse mt-ND1 were 5'-ATGCCAACCTCTTACTCT-3' (forward) and 5'-GCGGTGATGTAGAGGTGAT-3'

(reverse). The primer sequences used for amplifying mouse mt-ND6 were 5'-CCAATAGGATCCTCCCGAAT-3' (forward) and 5'-AGGTAGGATTGGTGTCTGG-3' (reverse). The primer sequences used for β -globin were 5'-CTATGGGACGCTTGATGT-3' (forward) and 5'-GCAATCATTCGTCTGTTT-3' (reverse).

Western blotting

Two lacrimal glands of one mouse were collected and pooled as one sample and homogenized in RIPA buffer. The protein samples (30 μ g each sample) were separated on SDS-PAGE gels and transferred to PVDF membranes (Merck-Merck-millipore, #IPVH00010). After blocking in 5% BSA, the membranes were incubated with Ucp1 (1:1000, CST, #14670S), Ucp2 (1:1000, CST, #89326), Ucp3 (1:1000, Novus, NBP2-24608), ChAT (1:1000, Abcam, ab178850) overnight at 4 °C and then HRP-conjugated goat anti-rabbit IgG at room temperature (1:3000, Zsbio, #ZB-2301). The bands were visualized using the ECL kit (Merck-millipore, #WBKLS0500) via enzyme-linked chemiluminescence and analyzed by Image J software (NIH).

Adrenalectomy (ADX)

After anesthesia and disinfection, a 0.5 cm incision was made on the back, followed by a 2 mm incision above each adrenal gland. The glands were removed with sterile forceps, the incisions were closed with staples, and 0.9% saline was injected subcutaneously to restore body fluid. Mice were provided with 0.9% NaCl as drinking water. The Sham group underwent the same procedure without adrenalectomy. Experiments were conducted 2 weeks after ADX.

Noradrenaline and acetylcholine measurement

Noradrenaline levels in the lacrimal gland and plasma were assessed using ELISA kits from Abnova (#KA3836 for lacrimal gland, #KA1891 for plasma), following the manufacturer's instructions. Acetylcholine (ACh) levels in the lacrimal gland were measured using ELISA kit from Abcam (# ab287812).

Mitochondrial stress testing

Lacrimal gland cells were isolated with 2 mg/ml collagenase II (Sigma, #C6885). After removing blood cells, 3×10^4 lacrimal gland cells with viability $\geq 85\%$ were seeded onto the Cell-Tak (Corning, #354240) coated XF8-well microplates (Agilent Technologies) with low buffered assay medium (Agilent Technologies) supplemented with 10 mM glucose, 1 mM sodium pyruvate and 2 mM Glutamine, pH 7.4. Oxygen consumption rate (OCR) was measured using a Seahorse XFp Flux Analyzer and XF cell mito stress test kit (Agilent Technologies)⁷⁵. Basal respiration was measured before injecting oligomycin at 1.5 μ M (final concentration). FCCP was then injected at 0.5 μ M (final concentration). Finally, a mixture of rotenone and antimycin A (at a 0.5 μ M final concentration) was injected. Mitochondrial basal respiration, proton leak, spare capacity and maximal respiration were measured after correcting for non-mitochondrial respiration. After finishing the test, 20 μ l of cell lysis buffer were added per well and protein content was measured using a BCA assay (Beyotime, #P0012). OCR rates were normalized to the protein content and presented as pmolesO₂/minute/ μ g protein.

Tissue processing and single-nucleus RNA sequencing (snRNA-seq)

Six lacrimal glands were obtained from C57BL/6J mice for each experiment. Tissue was chopped and homogenized with Nuclei EZ Lysis Buffer (NUC101; Sigma-Aldrich, St. Louis, MO, USA), then filtered through a 40 μ m cell strainer. After centrifugation at 500 g for 5 minutes at 4 °C, the pellet was resuspended in PBS. Red fluorescent protein (RFP)⁺ nuclei were collected individually in a 384 well plate for either Smart-seq2 or 10x Genomics sequencing after resuspension in the MoFlo Astrios EQ Cell Sorter (Beckman Coulter, Brea, CA, USA).

Following isolation, 2,5000 nuclei were placed into a 10x Genomics Chromium controller (PN110203; 10x Genomics, Pleasanton, CA, USA). Libraries were sequenced on an Illumina NovaSeq 6000 (20012850; 10x Genomics), and transcriptome data were aligned to the reference genome using the 10x Genomics Cell Ranger 3.1.0 pipeline. The data were imported into Seurat R 4.4.0 for quality control, excluding cells with fewer than 500 detected genes or over 10% mitochondrial gene expression, and filtering out genes expressed in fewer than three cells. Potential doublets were identified with DoubletFinder 2.0.4, adjusting the bimodality coefficient and artificial doublets to 0.25. For subsequent data analysis, canonical correlation analysis mitigated batch effects, and the LogNormalize method was applied for normalization. Principal component analysis (PCA) was performed on highly variable genes to facilitate cell clustering, followed by clustering at a resolution of 0.5 using “FindNeighbors” and “FindClusters”. This process yields fifteen unsupervised cell clusters. Clustering results were visualized with t-distributed stochastic neighbor embedding (t-SNE). Cell types were annotated using cluster-specific marker genes with “FindMarkers”. Immune cells were defined by the expression of PTPRC (also known as CD45) following a similar analytical approach.

Statistical analysis

All experiments were performed with at least three biological replicates, and each biological replicate contained three technical replicates. Data are presented as mean \pm SEM from at least three independent experiments. Statistical analysis was performed using GraphPad Prism 8.0. Statistical significance between two groups was determined by Mann-Whitney *U* test or unpaired Student's *t*-test, as appropriate. For multiple group comparisons, statistical significance was evaluated using One-way ANOVA followed by Dunnett's test. *P* values < 0.05 were considered statistically significant.

Reporting summary

Further information on research design is available in the Nature Portfolio Reporting Summary linked to this article.

Data availability

Bulk RNA-seq data are available in GEO under accession number [GSE224484](https://www.ncbi.nlm.nih.gov/geo/query/acc.cgi?acc=GSE224484), and snRNA-seq data under [GSE280211](https://www.ncbi.nlm.nih.gov/geo/query/acc.cgi?acc=GSE280211). All other data are included in the article or Supplementary Materials. Source data underlying all graphs are provided in the accompanying Source Data file. Source data are provided with this paper. All information is also available from the corresponding author upon request. Source data are provided with this paper.

Code availability

The code used for snRNA-seq analysis is available at GitHub (<https://github.com/LiXiaoyu1014/snRNA-analysis-of-SCOP-sample/tree/main>), based on R (version 4.3.2), and has been archived in Zenodo⁸³ with the <https://doi.org/10.5281/zenodo.15307689>.

References

- Zhou, L. & Beuerman, R. W. Tear analysis in ocular surface diseases. *Prog. Retin. Eye Res.* **31**, 527–550 (2012).
- Ohashi, Y., Dogru, M. & Tsubota, K. Laboratory findings in tear fluid analysis. *Clin. Chim. Acta* **369**, 17–28 (2006).
- Willcox, M. D. P. et al. TFOS DEWS II tear film report. *Ocul. Surf.* **15**, 366–403 (2017).
- Pflugfelder, S. C. & Stern, M. E. Biological functions of tear film. *Exp. Eye Res.* **197**, 108115 (2020).
- Rattner, A., Heng, J. S., Winer, B. L., Goff, L. A. & Nathans, J. Normal and Sjögren's syndrome models of the murine lacrimal gland studied at single-cell resolution. *Proc. Natl Acad. Sci. USA* **120**, e2311983120 (2023).
- Bannier-Helaouet, M. et al. Exploring the human lacrimal gland using organoids and single-cell sequencing. *Cell Stem Cell* **28**, 1221–1232.e1227 (2021).
- Toth-Molnar, E. & Ding, C. New insight into lacrimal gland function: Role of the duct epithelium in tear secretion. *Ocul. Surf.* **18**, 595–603 (2020).
- Dartt, D. A. Neural regulation of lacrimal gland secretory processes: relevance in dry eye diseases. *Prog. Retin. Eye Res.* **28**, 155–177 (2009).
- Nakamura, S. et al. The oxytocin system regulates tearing. *bioRxiv*, 2022.2003.2008.483433 (2022).
- Murata, K. et al. Increase of tear volume in dogs after reunion with owners is mediated by oxytocin. *Curr. Biol.* **32**, R869–R870 (2022).
- Jin, K. et al. Identification of lacrimal gland postganglionic innervation and its regulation of tear secretion. *Am. J. Pathol.* **190**, 1068–1079 (2020).
- Cuthbertson, S. et al. Localization of preganglionic neurons that innervate choroidal neurons of pterygopalatine ganglion. *Invest. Ophthalmol. Vis. Sci.* **44**, 3713–3724 (2003).
- Toth, I. E., Boldogkoi, Z., Medveczky, I. & Palkovits, M. Lacrimal preganglionic neurons form a subdivision of the superior salivatory nucleus of rat: transneuronal labelling by pseudorabies virus. *J. Auton. Nerv. Syst.* **77**, 45–54 (1999).
- Yeh, S. et al. Apoptosis of ocular surface cells in experimentally induced dry eye. *Invest. Ophthalmol. Vis. Sci.* **44**, 124–129 (2003).
- Yang, X. et al. IFN-gamma facilitates corneal epithelial cell pyroptosis through the JAK2/STAT1 pathway in dry eye. *Invest. Ophthalmol. Vis. Sci.* **64**, 34 (2023).
- Craig, J. P. et al. TFOS DEWS II definition and classification report. *Ocul. Surf.* **15**, 276–283 (2017).
- Clayton, J. A. Dry Eye. *N. Engl. J. Med.* **378**, 2212–2223 (2018).
- Stapleton, F. et al. TFOS DEWS II epidemiology report. *Ocul. Surf.* **15**, 334–365 (2017).
- Goto, E. et al. Tear evaporation rates in Sjögren's syndrome and non-Sjögren dry eye patients. *Am. J. Ophthalmol.* **144**, 81–85 (2007).
- Belmonte, C. et al. TFOS DEWS II pain and sensation report. *Ocul. Surf.* **15**, 404–437 (2017).
- Achtsidis, V. et al. Dry eye syndrome in subjects with diabetes and association with neuropathy. *Diabetes Care* **37**, e210–e211 (2014).
- Pflugfelder, S. C. et al. Nicotinic acetylcholine receptor stimulation: A new approach for stimulating tear secretion in dry eye disease. *Ocul. Surf.* **25**, 58–64 (2022).
- Nau, J., Wyatt, D. J., Rollema, H. & Crean, C. S. A phase I, open-label, randomized, 2-way crossover study to evaluate the relative bioavailability of intranasal and oral varenicline. *Clin. Ther.* **43**, 1595–1607 (2021).
- Wirta, D. et al. Efficacy and safety of OC-01 (varenicline solution) nasal spray on signs and symptoms of dry eye disease: the onset-2 phase 3 randomized trial. *Ophthalmology* **129**, 379–387 (2022).
- Wirta, D. et al. ONSET-1 phase 2b randomized trial to evaluate the safety and efficacy of oc-01 (varenicline solution) nasal spray on signs and symptoms of dry eye disease. *Cornea* **41**, 1207–1216 (2022).
- Frampton, J. E. Varenicline solution nasal spray: a review in dry eye disease. *Drugs* **82**, 1481–1488 (2022).
- Ding, C., Walcott, B. & Keyser, K. T. Sympathetic neural control of the mouse lacrimal gland. *Invest. Ophthalmol. Vis. Sci.* **44**, 1513–1520 (2003).
- Ding, C., Walcott, B. & Keyser, K. T. The alpha1- and beta1-adrenergic modulation of lacrimal gland function in the mouse. *Invest. Ophthalmol. Vis. Sci.* **48**, 1504–1510 (2007).
- Tangkrisanavinont, V. Stimulation of lacrimal secretion by sympathetic nerve impulses in the rabbit. *Life Sci.* **34**, 2365–2371 (1984).
- Meneray, M. A. & Fields, T. Y. Adrenergic stimulation of lacrimal protein secretion is mediated by G(q/11)alpha and G(s)alpha. *Curr. Eye Res.* **21**, 602–607 (2000).

31. Ota, I. et al. Alpha 1-adrenergic and cholinergic agonists activate MAPK by separate mechanisms to inhibit secretion in lacrimal gland. *Am. J. Physiol. Cell Physiol.* **284**, C168–C178 (2003).
32. Szarka, D. et al. Alpha-adrenergic agonists stimulate fluid secretion in lacrimal gland ducts. *Invest. Ophthalmol. Vis. Sci.* **61**, 3 (2020).
33. Li, W., Germain, R. N. & Gerner, M. Y. High-dimensional cell-level analysis of tissues with Ce3D multiplex volume imaging. *Nat. Protoc.* **14**, 1708–1733 (2019).
34. Scott-Solomon, E., Boehm, E. & Kuruvilla, R. The sympathetic nervous system in development and disease. *Nat. Rev. Neurosci.* **22**, 685–702 (2021).
35. Ceci, F. M. et al. Nerve growth factor in alcohol use disorders. *Curr. Neuropharmacol.* **19**, 45–60 (2021).
36. Hiltunen, P. H. & Airaksinen, M. S. Sympathetic cholinergic target innervation requires GDNF family receptor GFR alpha 2. *Mol. Cell. Neurosci.* **26**, 450–457 (2004).
37. Skaper, S. D. Neurotrophic factors: an overview. *Methods Mol. Biol.* **1727**, 1–17 (2018).
38. Cardoso, F. et al. Neuro-mesenchymal units control ILC2 and obesity via a brain-adipose circuit. *Nature* **597**, 410–414 (2021).
39. Kovács, I. et al. Substance P released from sensory nerve endings influences tear secretion and goblet cell function in the rat. *Neuropeptides* **39**, 395–402 (2005).
40. Smith-Edwards, K. M. et al. Sympathetic input to multiple cell types in mouse and human colon produces region-specific responses. *Gastroenterology* **160**, 1208–1223.e1204 (2021).
41. Hodges, R. R. et al. Nitric oxide and cGMP mediate alpha1D-adrenergic receptor-Stimulated protein secretion and p42/p44 MAPK activation in rat lacrimal gland. *Invest. Ophthalmol. Vis. Sci.* **46**, 2781–2789 (2005).
42. Chen, L. et al. Effects of alpha1D-adrenergic receptors on shedding of biologically active EGF in freshly isolated lacrimal gland epithelial cells. *Am. J. Physiol. -Cell Physiol.* **291**, C946–C956 (2006).
43. Robson-Doucette, C. A. et al. Beta-cell uncoupling protein 2 regulates reactive oxygen species production, which influences both insulin and glucagon secretion. *Diabetes* **60**, 2710–2719 (2011).
44. Diao, J. et al. UCP2 is highly expressed in pancreatic alpha-cells and influences secretion and survival. *Proc. Natl Acad. Sci. USA* **105**, 12057–12062 (2008).
45. Conti, B. et al. Transgenic mice with a reduced core body temperature have an increased life span. *Science* **314**, 825–828 (2006).
46. Toda, C. et al. UCP2 regulates mitochondrial fission and ventromedial nucleus control of glucose responsiveness. *Cell* **164**, 872–883 (2016).
47. Kong, D. et al. Glucose stimulation of hypothalamic MCH neurons involves K(ATP) channels, is modulated by UCP2, and regulates peripheral glucose homeostasis. *Cell Metab.* **12**, 545–552 (2010).
48. Poe, G. R. et al. Locus coeruleus: a new look at the blue spot. *Nat. Rev. Neurosci.* **21**, 644–659 (2020).
49. Lasagni Vitar, R. M., Fonteyne, P., Chaabane, L., Rama, P. & Ferrari, G. A hypothalamic-controlled neural reflex promotes corneal inflammation. *Invest. Ophthalmol. Vis. Sci.* **62**, 21 (2021).
50. Stern, M. E., Gao, J., Siemasko, K. F., Beuerman, R. W. & Pflugfelder, S. C. The role of the lacrimal functional unit in the pathophysiology of dry eye. *Exp. Eye Res.* **78**, 409–416 (2004).
51. Brinton, M. et al. Enhanced Tearing by electrical stimulation of the anterior ethmoid nerve. *Invest. Ophthalmol. Vis. Sci.* **58**, 2341–2348 (2017).
52. Bylsma, L. M., Gracani, A. & Vingerhoets, A. The neurobiology of human crying. *Clin. Auton. Res.* **29**, 63–73 (2019).
53. Bikbov, M. M. et al. The prevalence of dry eye in a very old population. *Acta Ophthalmol.* **100**, 262–268 (2022).
54. Balasubramanian, P., Hall, D. & Subramanian, M. Sympathetic nervous system as a target for aging and obesity-related cardiovascular diseases. *GeroScience* **41**, 13–24 (2019).
55. Rahbani, J. F. et al. ADRA1A-Gα(q) signalling potentiates adipocyte thermogenesis through CKB and TNAP. *Nat. Metab.* **4**, 1459–1473 (2022).
56. Li, J. et al. Monoamine oxidase A suppresses hepatocellular carcinoma metastasis by inhibiting the adrenergic system and its transactivation of EGFR signaling. *J. Hepatol.* **60**, 1225–1234 (2014).
57. Zhang, J., Simpson, P. C. & Jensen, B. C. Cardiac α1A-adrenergic receptors: emerging protective roles in cardiovascular diseases. *Am. J. Physiol. -Heart Circ. Physiol.* **320**, H725–h733 (2021).
58. Diano, S. & Horvath, T. L. Mitochondrial uncoupling protein 2 (UCP2) in glucose and lipid metabolism. *Trends Mol. Med.* **18**, 52–58 (2012).
59. Arsenijevic, D. et al. Disruption of the uncoupling protein-2 gene in mice reveals a role in immunity and reactive oxygen species production. *Nat. Genet.* **26**, 435–439 (2000).
60. Kim, J. D., Yoon, N. A., Jin, S. & Diano, S. Microglial UCP2 mediates inflammation and obesity induced by high-fat feeding. *Cell Metab.* **30**, 952–962.e955 (2019).
61. Li, E. et al. Control of lipolysis by a population of oxytocinergic sympathetic neurons. *Nature* **625**, 175–180 (2024).
62. Higashikuni, Y. et al. NLRP3 inflammasome activation through heart-brain interaction initiates cardiac inflammation and hypertrophy during pressure overload. *Circulation* **147**, 338–355 (2023).
63. Chakroborty, D. et al. Dopamine stabilizes tumor blood vessels by up-regulating angiopoietin 1 expression in pericytes and Kruppel-like factor-2 expression in tumor endothelial cells. *Proc. Natl Acad. Sci. USA* **108**, 20730–20735 (2011).
64. O’Neil, E. C., Henderson, M., Massaro-Giordano, M. & Bunya, V. Y. Advances in dry eye disease treatment. *Curr. Opin. Ophthalmol.* **30**, 166–178 (2019).
65. Tauber, J. et al. NOV03 for dry eye disease associated with meibomian gland dysfunction: results of the randomized phase 3 GOBI study. *Ophthalmology* **130**, 516–524 (2023).
66. Sheppard, J. D. et al. NOV03 for signs and symptoms of dry eye disease associated with meibomian gland dysfunction: the randomized phase 3 MOJAVE study. *Am. J. Ophthalmol.* **252**, 265–274 (2023).
67. Tian, L. et al. Perfluorohexyloctane eye drops for dry eye disease associated with meibomian gland dysfunction in chinese patients: a randomized clinical trial. *JAMA Ophthalmol.* **141**, 385–392 (2023).
68. Lepor, H., Kazzazi, A. & Djavan, B. α-Blockers for benign prostatic hyperplasia: the new era. *Curr. Opin. Urol.* **22**, 7–15 (2012).
69. Assad Kahn, S. et al. The anti-hypertensive drug prazosin inhibits glioblastoma growth via the PKCδ-dependent inhibition of the AKT pathway. *EMBO Mol. Med.* **8**, 511–526 (2016).
70. Esler, M. D. et al. Renal sympathetic denervation in patients with treatment-resistant hypertension (The Symplicity HTN-2 Trial): a randomised controlled trial. *Lancet* **376**, 1903–1909 (2010).
71. Vaseghi, M. et al. Cardiac sympathetic denervation for refractory ventricular arrhythmias. *J. Am. Coll. Cardiol.* **69**, 3070–3080 (2017).
72. Habbe, N. et al. Spontaneous induction of murine pancreatic intraepithelial neoplasia (mPanIN) by acinar cell targeting of oncogenic Kras in adult mice. *Proc. Natl Acad. Sci. USA* **105**, 18913–18918 (2008).
73. Masli, S. & Dartt, D. A. Mouse models of Sjögren’s syndrome with ocular surface disease. *Int. J. Mol. Sci.* **21** (2020).
74. Qu, M. et al. Therapeutic effects of stat3 inhibition on experimental murine dry eye. *Invest. Ophthalmol. Vis. Sci.* **60**, 3776–3785 (2019).
75. Qu, M. et al. Hyperglycemia-induced severe mitochondrial bioenergetic deficit of lacrimal gland contributes to the early onset of dry eye in diabetic mice. *Free Radic. Biol. Med.* **166**, 313–323 (2021).
76. Xue, Y. et al. The mouse autonomic nervous system modulates inflammation and epithelial renewal after corneal abrasion through the activation of distinct local macrophages. *Mucosal Immunol.* **11**, 1496–1511 (2018).

77. Chen, K. et al. Irisin protects mitochondria function during pulmonary ischemia/reperfusion injury. *Sci. Transl. Med.* **9** eaao6298 (2017).
78. Cock, P. J., Fields, C. J., Goto, N., Heuer, M. L. & Rice, P. M. The Sanger FASTQ file format for sequences with quality scores, and the Solexa/Illumina FASTQ variants. *Nucleic Acids Res.* **38**, 1767–1771 (2010).
79. Langmead, B. & Salzberg, S. L. Fast gapped-read alignment with Bowtie 2. *Nat. Methods* **9**, 357–359 (2012).
80. Li, B. & Dewey, C. N. RSEM: accurate transcript quantification from RNA-Seq data with or without a reference genome. *BMC Bioinforma.* **12**, 323 (2011).
81. Yu, G., Wang, L. G., Han, Y. & He, Q. Y. clusterProfiler: an R package for comparing biological themes among gene clusters. *OMICS* **16**, 284–287 (2012).
82. Li, P., Ni, S., Zhang, L., Zeng, S. & Luo, Q. Imaging cerebral blood flow through the intact rat skull with temporal laser speckle imaging. *Opt. Lett.* **31**, 1824–1826 (2006).
83. Qu, M. et al. Code for “A gatekeeper sympathetic control of lacrimal tear secretion and dry eye onset through the NA-Adra1a-Ucp2 pathway”. *Zenodo*. <https://doi.org/10.5281/zenodo.15307689> (2025).

Acknowledgements

We acknowledge Prof. Kazuo Tsubota (Keio University), Prof. Chuanqing Ding (University of Southern California), Prof. Haiwei Xu and Prof. Xiaotang Fan (Army Medical University), Prof. Wei Li (Xiamen University), and Prof. Guichang Zou (Shandong First Medical University) for their critical reading and helpful suggestions regarding the manuscript. We thank Xiaoyu Li for providing the analysis of the snRNA-seq data. All the schematic diagrams are created with BioRender.com. This work was supported by Shandong Provincial Key Research and Development Program (Grant no. 2021ZDSYS14 to L.X.), Joint Innovation Team for Clinical & Basic Research (Grant no. 202405 to L.X.), Taishan Scholar Program (Grant no. tstp20221163 to Q.Z.), and the Natural Science Foundation of Shandong Province (Grant no. ZR2022MH033 to M.Q.).

Author contributions

Q.Z. and L.X. conceptualized, acquired funding, and supervised this study. M.Q., Q.W., X.B., J.F., Y.Z., Q.C., H.Z., Q.G. and H.W. performed data acquisition, analysis and interpretation. Sequencing data were processed and analyzed by B.Z., and S.D. Immunohistochemical experiments were performed by S.Z. and Y.Q. Y.C. provided advice and discussed results. The manuscript was drafted by M.Q. and Q.W., and reviewed and edited by Q.Z., L.X., and Y.C. All authors read, edited, and approved the final manuscript. M.Q. and Q.W. are co-first authors, with M.Q. listed first because of her major contributions regarding experiment design and manuscript preparation.

Competing interests

A Chinese patent (ZL202210497086.8) has been granted to Eye Institute of Shandong First Medical University (Shandong Eye Institute, Qingdao Eye Hospital of Shandong First Medical University), with inventors Lixin Xie, Qingjun Zhou, Mingli Qu, and Sai Zhang. It covers the use of sympathetic activation inhibitors and/or α 1-adrenergic receptor antagonists for treating dry eye. A related PCT application (PCT/CN2022/113244) is under examination. All other authors declare no competing interests.

Additional information

Supplementary information The online version contains supplementary material available at <https://doi.org/10.1038/s41467-025-60476-z>.

Correspondence and requests for materials should be addressed to Lixin Xie or Qingjun Zhou.

Peer review information *Nature Communications* thanks Anny Cheng, Kazuo Tsubota and the other anonymous reviewer(s) for their contribution to the peer review of this work. A peer review file is available.

Reprints and permissions information is available at <http://www.nature.com/reprints>

Publisher's note Springer Nature remains neutral with regard to jurisdictional claims in published maps and institutional affiliations.

Open Access This article is licensed under a Creative Commons Attribution-NonCommercial-NoDerivatives 4.0 International License, which permits any non-commercial use, sharing, distribution and reproduction in any medium or format, as long as you give appropriate credit to the original author(s) and the source, provide a link to the Creative Commons licence, and indicate if you modified the licensed material. You do not have permission under this licence to share adapted material derived from this article or parts of it. The images or other third party material in this article are included in the article's Creative Commons licence, unless indicated otherwise in a credit line to the material. If material is not included in the article's Creative Commons licence and your intended use is not permitted by statutory regulation or exceeds the permitted use, you will need to obtain permission directly from the copyright holder. To view a copy of this licence, visit <http://creativecommons.org/licenses/by-nc-nd/4.0/>.

© The Author(s) 2025